

Electronic Supplemental Material

Exfoliated Two-dimensional Bimetallic Ni_{0.6}Co_{0.4}-Metal Organic Framework Nanosheets with Mixed Ligands for Enhanced Acid Electrocatalytic Water Oxidation

Wensheng Liu^{a,‡} Xinke Hu^{a,‡} KaiQiang Zeng^a, Chen-Hui Ji^{*,a,b}, Hui Feng^c and Qing-Yun Cai^{*,a}

a. State Key Laboratory of Chemo/Biosensing and Chemometrics, College of Chemistry and Chemical Engineering, Hunan University, Changsha 410082, China

b. Department of Chemistry, Baotou Teachers' College, Baotou 014030, China

c. Changsha Environmental Protection College, Hunan Province, Changsha 410082, China

E-mail: qycail0001@hnu.edu.cn, jich@hnu.edu.cn

‡Wensheng Liu and Xinke Hu equally contributed to this work.

Experimental section

Materials and reagents

1,2-Benzenediacetic acid (H_2BEC , $\geq 99\%$), imidazole ($\geq 99\%$), 4,4'-dibromobiphenyl ($\geq 98\%$) purchased from Shanghai Aladdin Biochemical Technology Co., Ltd. Sulfuric acid (98%, GR), anhydrous potassium carbonate (K_2CO_3), anhydrous copper sulfate ($CuSO_4$) purchased from Beijing Sinopath Group Chemical Reagents Co., Ltd. Ethanol, methanol, $Co(NO_3)_2 \cdot 6H_2O$, $Ni(ClO_4)_2 \cdot 6H_2O$, N,N-dimethylformamide (DMF), ethyl acetate, dimethyl sulfoxide, N-methylpyrrolidone (NMP), isopropyl alcohol and acetone were purchased from Shanghai Macklin Biochemical Technology Co., Ltd. These reagents were purchased and used from the market without further purification. The ultrapure water used in the experiments was obtained from Wahaha Group Co Ltd, Hangzhou, China, and was not further purified

Instrumentation

Single crystal diffraction data (XRD) of Co-MOF (273.15 K), Ni-MOF (273 (2) K), and $Ni_{0.6}Co_{0.4}$ -MOF (150.15 K) were collected using Mo $K\alpha$ radiation ($\lambda=0.71073$) on a Brooke D8 Quest X-ray single crystal diffractometer to determine the structure. Then, using Olex2-1.5 and the SHELX package, refinement was performed on F^2 using full matrix least squares technique. The powder X-ray diffraction data (p-XRD) of Co-MOF, Ni-MOF, and $Ni_{0.6}Co_{0.4}$ -MOF were tested using Cu $K\alpha$ radiation on a Panaco Empyren diffractometer. The thermogravimetric analysis (TGA) data of Co-MOF, Ni-MOF, and $Ni_{0.6}Co_{0.4}$ -MOF crystals were performed and recorded on a NETZSCH STA2500 analyzer under N_2 atmosphere at a heating rate of $5\text{ }^\circ\text{C min}^{-1}$. X-ray photoelectron spectroscopy (XPS) was recorded on the Thermo Scientific Thermo Fisher Scientific K-Alpha X-ray photoelectron spectrometer. The Fourier transform infrared spectra (FTIR, KBr particles, $450\text{-}4000\text{cm}^{-1}$ region) of H_2BEC , BIBP, Co-MOF, Ni-MOF, and $Ni_{0.6}Co_{0.4}$ -MOF crystals were determined by utilizing the Thermo Fisher IS-50 Fourier transform infrared spectrometer. The ratio of metal

ions in Ni_{0.6}Co_{0.4}-MOF crystals was quantified via ICP-MS plasma mass spectrometer (NexION, PerkinElmer). Based on X-ray single crystal diffraction, TGA, FT-IR, and XPS, the crystallographic data of Co MOF, Ni MOF, and Ni_{0.6}Co_{0.4}-MOF can be best displayed (Table 1), and the obtained bond distances and bond angles are shown in Tables S1-S4 and S6. The CCDC number for Co-MOF/Ni-MOF/Ni_{0.6}Co_{0.4}-MOF is 2341403/2342678/2347597. These codes contain detailed crystallographic data and serve as a follow-up supplement to the structure of this article. These crystal data can be obtained from the Cambridge Crystallographic Data Center (<https://www.ccdc.cam.ac.uk>). Nanosheets were prepared by ultrasonic exfoliation of Co-MOF, Ni-MOF, and Ni_{0.6}Co_{0.4}-MOF crystal blocks using the cell disruptor (SN-PF2). The morphological evolution of Co-MOF, Ni-MOF, and Ni_{0.6}Co_{0.4}-MOF before and after exfoliation into nanosheets was observed and recorded using the TESCAN high-resolution scanning electron microscope (SEM). The internal morphology of nanosheets formed by the exfoliation of Co-MOF, Ni-MOF, and Ni_{0.6}Co_{0.4}-MOF was verified by utilising the Japanese electronic JEOL F200 transmission electron microscope. The electrocatalytic water oxidation behavior of Co-MOF, Ni-MOF, Ni_{0.6}Co_{0.4}-MOF and their composite materials was recorded using the Chenhua CHI660D electrochemical workstation. Electrochemical impedance spectra were recorded in AutoLab (AUT88125).

Synthesis of ligand 4, 4'-bisimidazolylbiphenyl (BIBP)

The synthetic strategy was based on literature S1 and was briefly adapted. The reaction process is shown in Figure S1. In short, 4, 4' - dibromobiphenyl (12.5 g, 0.04 mol), imidazole (11.5 g, 0.16 mol), anhydrous potassium carbonate (17.97 g, 0.13 mol), and anhydrous copper sulfate (0.16 g, 1 mmol) were weighed and thoroughly grinded in a mortar and pestle until mixed thoroughly. The mixture was then transferred to a round-bottomed flask heated at 180 °C for 12 h under argon atmosphere. The mixture was cooled naturally to room temperature and washed with water. The residue was extracted five times with 100 mL of ethanol, the organic layer

was separated and transferred to a rotary evaporator for evaporation to obtain the crude product. Finally, the crude product was recrystallized utilizing methanol and water to obtain light brown powdery crystals. Yield: 53.2%. FT-IR (Figure 2d, KBr pellet, cm^{-1}): 3096(w), 1604(s), 1513(vs), 1296(vs), 1257(m), 1049(m), 958 (m), 897 (m), 819(s), 736(m) 654(m), 515(m). ^1H NMR (400 MHz, Chloroform-d, Figure S2) δ 7.92 (s, 2H), 7.72 (d, $J = 8.1$ Hz, 4H), 7.51 (d, $J = 8.1$ Hz, 4H), 7.35 (s, 2H), 7.26 (d, $J = 6.4$ Hz, 2H).

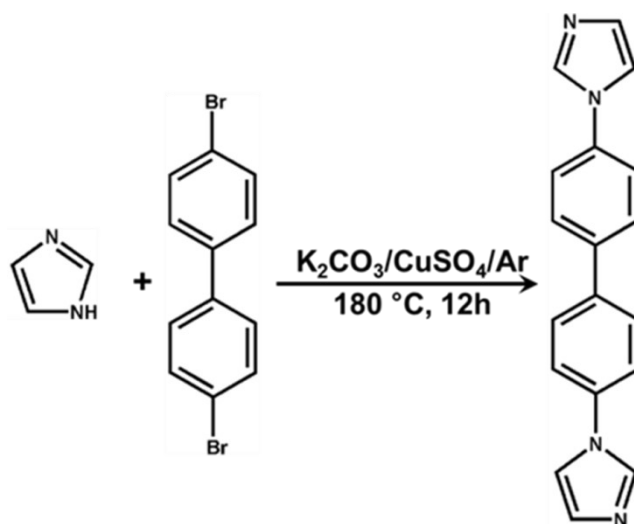


Fig. S1 Synthesis of BIBP.

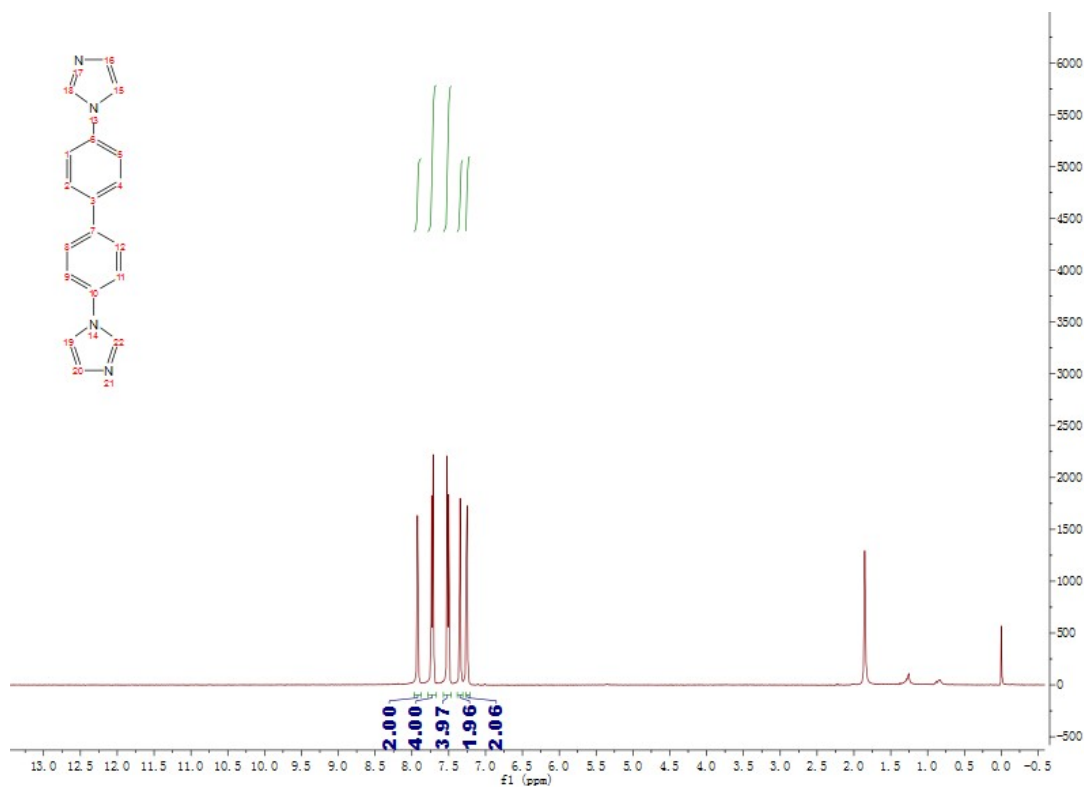


Fig. S2 ^1H NMR of BIBP.

Preparation of 3D Layered Co-MOF $[\text{Co}(\text{BEC})_2 (\text{BIBP})_2]_n$ Crystals

H_2BEC (0.2 mmol, 0.039 g) and BIBP (0.2 mmol, 0.042 g) were weighed and dissolved in 12 mL of mixed solvent (H_2O : DMF=5:1), respectively. The obtained dispersion was sonicated until completely dispersed. Then, $\text{Co}(\text{NO}_3)_2 \cdot 6\text{H}_2\text{O}$ (0.1 mmol, 0.0291 g) was added and stirred well until completely dissolved. The dissolved mixture is transferred to a PTFE liner and sealed completely with a stainless steel reactor. The reaction device was continuously heated at 110 °C for 72 hours, and then naturally cooled to room temperature to obtain purple block shaped crystals (Scheme S1, Fig. S5a and Fig. S5b). The crystals are repeatedly filtered 5-10 times using the mother liquor. The crystals are repeatedly filtered 5-10 times by using the mother liquor so as to remove residual organic matter and unreacted ions. After the purification procedure is completed it is placed in the mother liquor and stored at

room temperature. The yield is approximately 49.2% based on Co^{2+} . FTIR data (cm^{-1} , KBr pellet, Figure 2d): 3144 (w), 1700(w), 1612(s), 1517(vs), 1365(s), 1305(w), 1256(m), 1188(w), 1127(w), 1062 (m), 819(s), 728 (m), 658(m), 532(m), 485(m).

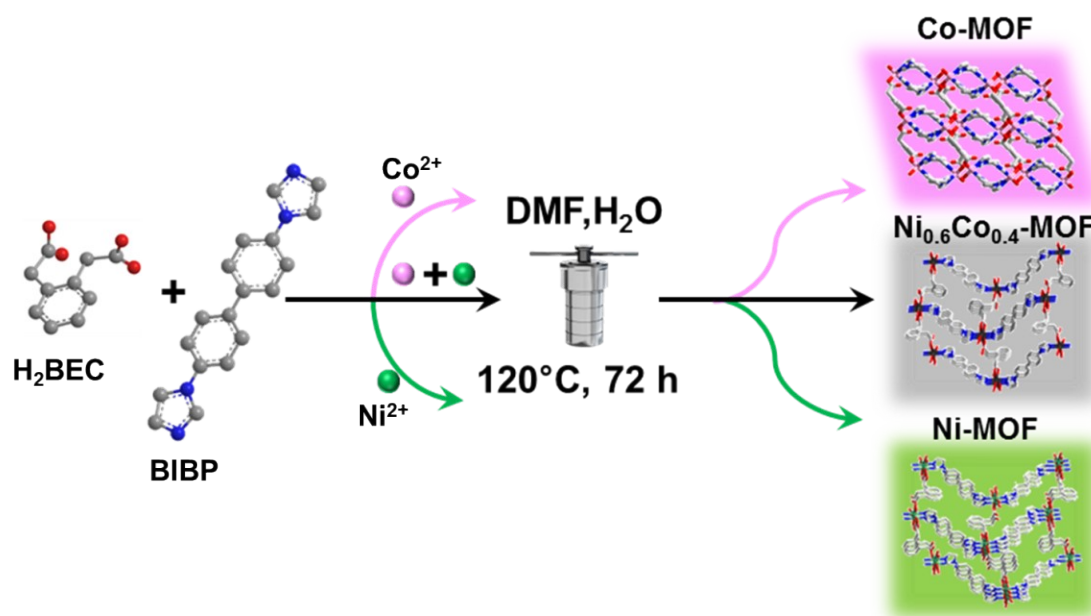
Preparation of 3D Layered Ni-MOF $[\text{Ni}(\text{BEC})_2(\text{BIBP})_2(\text{H}_2\text{O})]_n$ Crystals

H_2BEC (0.2 mmol, 0.039 g) and BIBP (0.2 mmol, 0.042 g) were weighed and dissolved in 12 mL of mixed solvent ($\text{H}_2\text{O}:\text{DMF}=5:1$), respectively. The obtained dispersion was sonicated until completely dispersed. Then, $\text{Ni}(\text{ClO}_4)_2 \cdot 6\text{H}_2\text{O}$ (0.1 mmol, 0.025759 g) was added and stirred well until completely dissolved. The dissolved mixture is transferred to a PTFE liner and sealed completely with a stainless steel reactor. The reaction device was continuously heated at 110 °C for 72 hours, and then naturally cooled to room temperature to obtain purple block shaped crystals (Scheme S1, Fig. S5c and Fig. S5d). The crystals are repeatedly filtered 5-10 times using the mother liquor. The crystals are repeatedly filtered 5-10 times by using the mother liquor so as to remove residual organic matter and unreacted ions. After the purification procedure is completed it is placed in the mother liquor and stored at room temperature. The yield is approximately 45.7% based on Ni^{2+} . Infrared data (cm^{-1} , KBr pellet, Figure 2d): 3383(br, w), 3118(w), 3053(w), 2939(w), 2818(br, w), 1713(w) 1517(s), 1417(m), 1378(m), 1300(m), 1261(m), 1200(w), 1140(w), 1058(s), 949(m), 866(w), 819(w), 724(m), 654(m), 584(w), 507(w), 415(vw) .

Preparation of 3D Layered $\text{Ni}_{0.6}\text{Co}_{0.4}$ -MOF Crystals $[\text{Ni}_{0.6}\text{Co}_{0.4} (\text{BEC})_2(\text{BIBP})_2(\text{H}_2\text{O})]_n$

H_2BEC (0.2 mmol, 0.039 g) and BIBP (0.2 mmol, 0.042 g) were weighed and dissolved in 12 mL of mixed solvent ($\text{H}_2\text{O}:\text{DMF}=5:1$), respectively. The obtained dispersion was sonicated until completely dispersed. Then, $\text{Co}(\text{NO}_3)_2 \cdot 6\text{H}_2\text{O}$ (0.05 mmol, 0.014552 g) and $\text{Ni}(\text{ClO}_4)_2 \cdot 6\text{H}_2\text{O}$ (0.05 mmol, 0.0128795 g) were added and

stirred well until completely dissolved. The dissolved mixture is transferred to a PTFE liner and sealed completely with a stainless steel reactor. The reaction device was continuously heated at 110 °C for 72 hours, and then naturally cooled to room temperature to obtain purple block shaped crystals (Scheme S1, Fig. S5e and Fig. S5f). The crystals are repeatedly filtered 5-10 times using the mother liquor. The crystals are repeatedly filtered 5-10 times by using the mother liquor so as to remove residual organic matter and unreacted ions. After the purification procedure is completed it is placed in the mother liquor and stored at room temperature. The yield is approximately 47.3% based on nickel ions. Infrared data (cm⁻¹, Figure 2d): 3313(br, w) 3117 (w), 3055(w), 2970 (w), 2823(w) 1681 (vw), 1554(m), 1519(s), 1379(s), 1303(m), 1256(m), 1188(m), 1135(w), 1062(m), 1004(m), 834(s), 721(s), 653(w), 588(w), 496(s).



Scheme S1. Schematic diagram of hydrothermal solvothermal synthesis of Co-MOF, Ni-MOF and Ni_{0.6}Co_{0.4}-MOF.

Exfoliation of thin MOF nanosheets by cell fragmentation

MOF bulk crystals (100 mg: Co-MOF, Ni-MOF, or Ni_{0.6}Co_{0.4}-MOF) were weighed and placed in a centrifuge tube containing 30 mL of NMP. The centrifuge

tube is then transferred and secured into a beaker filled with crushed ice. The beaker is placed in the cell disruptor and a probe capable of carrying various powers (60 W, 125 W, 250 W and 300 W) is then immersed in the centrifuge tube. The MOF bulk crystals were exfoliated for a specific time (10 min, 30 min and 60 min) and the obtained nanosheets were dispersed in NMP.

The obtained MOF nanosheets were collected by using multi-step centrifugation. First, the initial product was centrifuged in a centrifuge at 1000 r min^{-1} for 15 min. Then, the supernatant was taken and continued to be centrifuged at 3000 r min^{-1} for 15 min. Finally, the obtained MOF nanosheets (Co-MOF NHs, Ni-MOF NHs, or $\text{Ni}_{0.6}\text{Co}_{0.4}$ -MOF NHs) dispersion was refrigerated and set aside.

Preparation of catalyst ink

For MOF bulk crystals, gently tap and grind the block crystals until they are converted into fine powder, then mix 10 mg of fine catalyst powder, 20 μL of 1wt% Nafion, and 1.98 mL of 70% isopropanol solution by ultrasonic treatment for 60 minutes. The obtained dispersion is refrigerated for later use.

For MOF nanosheets, 10 mg of MOF nanosheets were directly weighed, and 20 μL of 1wt% Nafion and 1.98 mL of 70% isopropanol solution were sonicated for 60 minutes. The obtained dispersion was refrigerated for later use.

For $\text{Ni}_{0.6}\text{Co}_{0.4}$ -MOF NHs/CB, similar to the above procedure, only 30 mg of carbon black needs to be added during the process, followed by ultrasonic mixing treatment for 60 minutes, and the obtained dispersion is refrigerated for later use.

Preparation of working electrode

Carbon paper (1 cm \times 1 cm) was used as the electrode substrate. The prepared catalyst ink (400 μL) was transferred to carbon paper by drop casting method. It was then dried by intermittent heating using sodium lamp. Finally, the prepared electrode was dried at room temperature overnight.

Electrochemical testing

The OER catalytic activity was measured using a three electrode system at room temperature in an aqueous solution of 0.05 M H₂SO₄ (pH ≈ 1.3). The drop cast carbon paper serves as the working electrode, graphite rod as the counter electrode, and Ag/AgCl as the reference electrode. Before conducting the test, the electrode is scanned 20 times to stabilize the electrochemical response. Prior to the linear sweep voltammetry (LSV) test, a 5-cycle cyclic voltammetry test (0.2 V-1.95 V vs. Ag/AgCl, 50 mV s⁻¹) was performed to stabilize the response signal of the electrode. LSV measurement data was obtained using a scan rate of 5 mV s⁻¹ within the range of 0.2 V-1.95 V (vs. Ag/AgCl). Then use equation S1 to convert the potential to RHE standard:

$$E_{\text{RHE}} = E_{\text{Ag/AgCl}} + 0.197 + 0.0591\text{pH} \quad \text{S1}$$

Convert the current measurement value to current density by dividing by the geometric area of the working electrode (1 cm²). Calculate the overpotential η using equation S2:

$$\text{Overpotential } \eta = \text{Application test potential (V vs RHE)} - 1.23 \text{ V} \quad \text{S2}$$

Electrochemical Stability Tests Passed The following tests were verified for changes in LSV performance after 1000 cyclic voltammetry scans, chronopotentiometry (12h), high-resolution transmission electron microscopy and X-ray diffractometry.

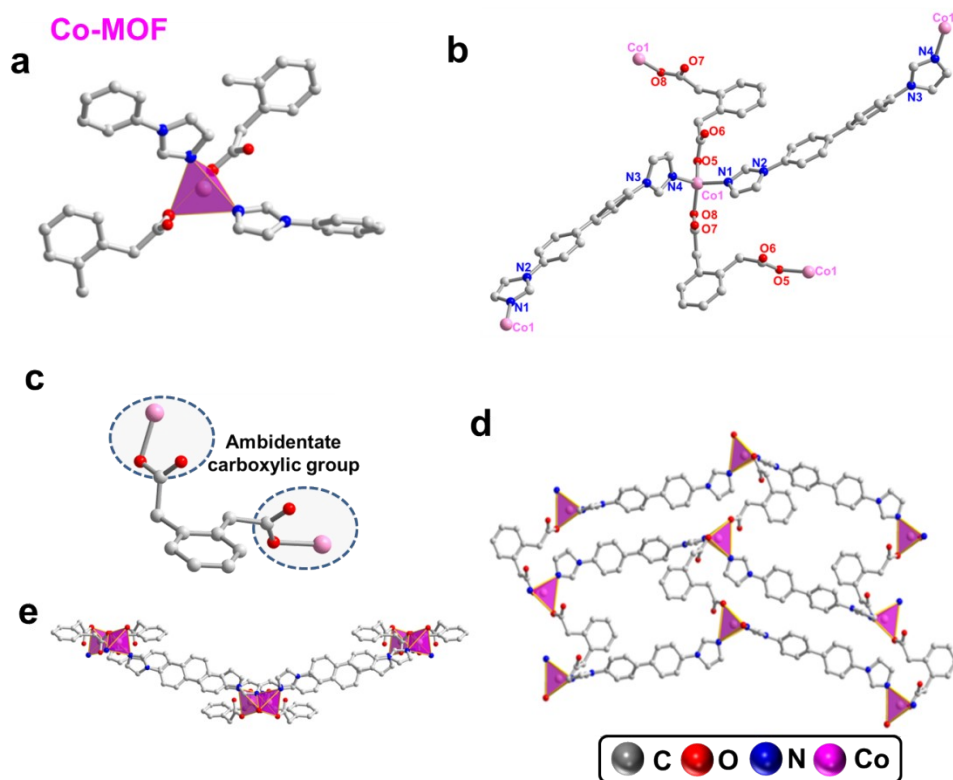


Fig. S3 Crystal structure of Co-MOF. (a) Asymmetric units of Co-MOF; (b) Coordination environment of central Co^{2+} in Co-MOF; (c) The coordination mode of carboxyl linking groups on ligand H_2BEC in Co-MOF; (d) The connection mode of organic ligands (H_2BEC and BIBP) along the b-axis direction; (e) 2D slice structure diagram along the c-axis. For clarity, the H atom has been removed.

Table S1. Bond lengths [\AA] and angles [$^\circ$] for Co-MOF.

Atom-Atom	Length/ \AA	Atom-Atom-Atom	Angle/ $^\circ$	Atom-Atom-Atom	Angle/ $^\circ$
Co1-O5	1.9749(11)	O5-Co1-O8 ¹	104.62(5)	N4-C16-N3	111.08(13)
Co1-O8 ¹	1.9911(11)	O5-Co1-N1	108.45(5)	C18-C17-N3	105.84(13)
Co1-N1	2.0150(12)	O5-Co1-N4 ²	112.02(5)	C17-C18-N4	109.69(13)
Co1-N4 ²	2.0219(12)	O8 ¹ -Co1-N1	108.98(5)	O5-C19-C20	115.79(14)
O5-C19	1.2890(19)	O8 ¹ -Co1-N4 ²	114.12(5)	O6-C19-O5	124.10(14)
O6-C19	1.235(2)	N1-Co1-N4 ²	108.47(5)	O6-C19-C20	120.10(14)
O7-C28	1.2341(19)	C19-O5-Co1	114.68(10)	C21-C20-C19	115.74(13)
O8-C28	1.2890(19)	C28-O8-Co1 ³	107.87(9)	C22-C21-C20	122.33(13)
N1-C1	1.3170(19)	C1-N1-Co1	126.70(10)	C22-C21-C26	118.63(14)
N1-C2	1.3739(19)	C1-N1-C2	105.91(12)	C26-C21-C20	119.02(13)
N2-C1	1.3490(19)	C2-N1-Co1	127.29(10)	C21-C22-C23	121.48(15)
N2-C3	1.381(2)	C1-N2-C3	106.53(12)	C24-C23-C22	119.81(16)
N2-C4	1.4293(18)	C1-N2-C4	126.50(12)	C23-C24-C25	119.46(15)
N3-C13	1.4327(18)	C3-N2-C4	126.96(13)	C24-C25-C26	121.42(15)
N3-C16	1.3476(18)	C16-N3-C13	124.45(12)	C21-C26-C27	121.36(13)
N3-C17	1.3836(19)	C16-N3-C17	107.48(12)	C25-C26-C21	119.20(15)
N4-C16	1.3216(19)	C17-N3-C13	127.86(12)	C25-C26-C27	119.44(14)
N4-C18	1.3828(19)	C16-N4-Co1 ⁴	124.31(10)	C26-C27-C28	114.60(13)
C2-C3	1.353(2)	C16-N4-C18	105.91(12)	O7-C28-O8	123.22(14)
C4-C5	1.383(2)	C18-N4-Co1 ⁴	128.76(10)	O7-C28-C27	120.77(14)
C4-C9	1.384(2)	N1-C1-N2	111.55(13)	O8-C28-C27	116.01(13)
C5-C6	1.385(2)	C3-C2-N1	109.55(14)		
C6-C7	1.393(2)	C2-C3-N2	106.46(14)		
C7-C8	1.393(2)	C5-C4-N2	119.53(13)		
C7-C10	1.484(2)	C5-C4-C9	119.86(14)		
C8-C9	1.386(2)	C9-C4-N2	120.61(13)		
C10-C11	1.398(2)	C4-C5-C6	119.65(15)		
C10-C15	1.393(2)	C5-C6-C7	121.56(15)		
C11-C12	1.379(2)	C6-C7-C8	117.70(14)		
C12-C13	1.385(2)	C6-C7-C10	120.86(14)		
C13-C14	1.385(2)	C8-C7-C10	121.35(14)		
C14-C15	1.391(2)	C9-C8-C7	121.13(15)		
C17-C18	1.357(2)	C4-C9-C8	120.00(14)		
C19-C20	1.523(2)	C11-C10-C7	118.90(14)		
C20-C21	1.519(2)	C15-C10-C7	122.83(14)		
C21-C22	1.391(2)	C15-C10-C11	118.23(14)		
C21-C26	1.407(2)	C12-C11-C10	121.44(15)		
C22-C23	1.393(2)	C11-C12-C13	119.01(15)		
C23-C24	1.381(3)	C12-C13-N3	118.09(13)		
C24-C25	1.385(3)	C14-C13-N3	120.58(13)		
C25-C26	1.397(2)	C14-C13-C12	121.32(14)		
C26-C27	1.504(2)	C13-C14-C15	118.85(14)		
C27-C28	1.529(2)	C14-C15-C10	121.14(14)		
¹ +X,2-Y,-1/2+Z; ² 1-X,1+Y,1/2-Z		¹ +X,2-Y,-1/2+Z; ² 1-X,1+Y,1/2-Z; ³ +X,2-Y,1/2+Z; ⁴ 1-X,-1+Y,1/2-Z			

Table S2. H-Bond lengths [\AA] and angles [$^\circ$] for **Co-MOF**.

Donor --- H....Acceptor	D - H	H...A	D...A	D - H...A
C2---H2....O7	0.93	2.54	3.075(2)	117
C3---H3....O6	0.93	2.60	3.423(2)	148
C12---H12....O8	0.93	2.46	3.349(2)	160
C16---H16....O7	0.93	2.42	2.912(2)	113
C18---H18....O6	0.93	2.55	3.191(2)	126
C20---H20B....O7	0.97	2.53	3.240(2)	130
C22---H22....O6	0.93	2.55	3.130(2)	121

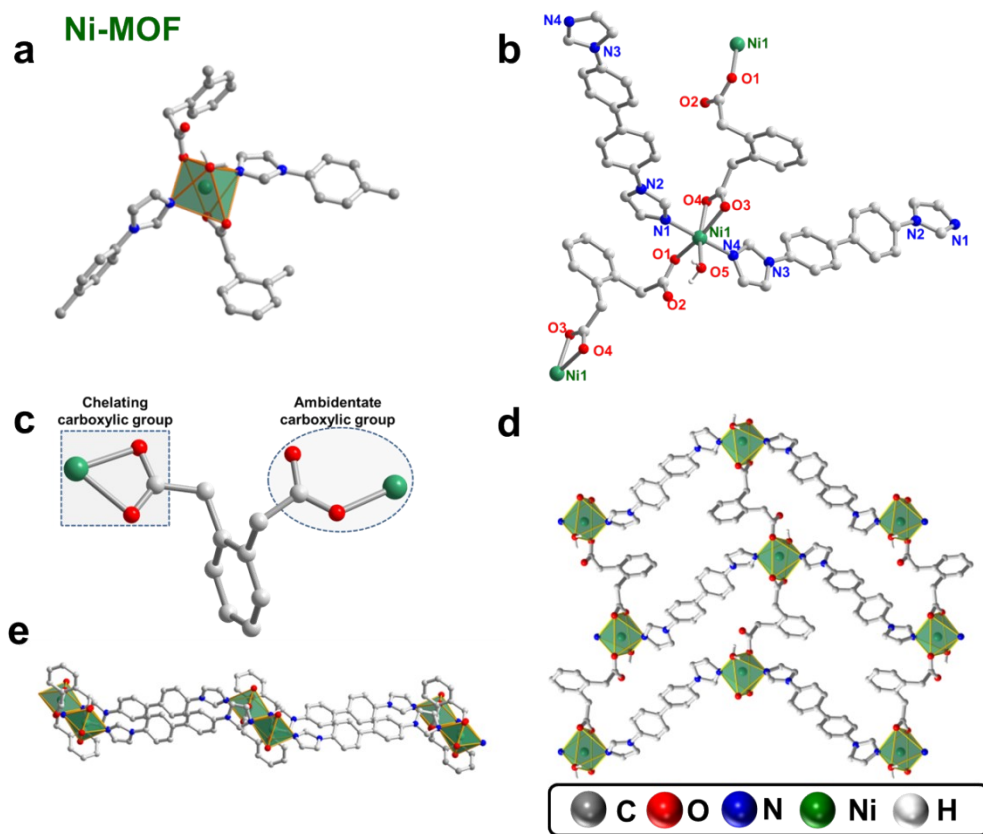


Fig. S4 Crystal structure of Ni-MOF. (a) Asymmetric unit of Ni-MOF; (b) Coordination environment of central Ni^{2+} in Ni-MOF; (c) Coordination mode of carboxyl linking group on ligand H_2BEC in Ni-MOF; (d) Connection mode of organic ligands (H_2BEC and BIBP); (e) 2D sheet structure diagram along the c -axis. For clarity, H atoms are removed.

Table S3. Bond lengths [\AA] and angles [$^\circ$] for Ni-MOF.

Atom-Atom	Length/ \AA	Atom-Atom-Atom	Angle/ $^\circ$	Atom-Atom-Atom	Angle/ $^\circ$
Ni1-O1	2.0713(10)	O1-Ni1-O3 ¹	163.45(4)	C1-N2-C3	107.13(12)
Ni1-O3 ¹	2.1598(10)	O1-Ni1-O4 ¹	101.37(4)	C1-N2-C4	125.55(13)
Ni1-O4 ¹	2.1120(11)	O1-Ni1-O5	96.71(4)	C3-N2-C4	127.24(13)
Ni1-O5	2.0841(11)	O1-Ni1-C28 ¹	132.47(5)	C16-N3-C13	127.20(13)
Ni1-N1	2.0528(13)	O3 ¹ -Ni1-C28 ¹	30.97(4)	C18-N3-C13	125.80(13)
Ni1-N4 ²	2.0515(13)	O4 ¹ -Ni1-O3 ¹	62.07(4)	C18-N3-C16	106.98(12)
Ni1-C28 ¹	2.4530(15)	O4 ¹ -Ni1-C28 ¹	31.10(4)	C17-N4-Ni1 ⁴	126.57(10)
O1-C19	1.2712(19)	O5-Ni1-O3 ¹	99.84(4)	C18-N4-Ni1 ⁴	127.07(10)
O2-C19	1.249(2)	O5-Ni1-O4 ¹	161.89(4)	C18-N4-C17	106.36(13)
O3-C28	1.2637(18)	O5-Ni1-C28 ¹	130.82(5)	N1-C1-N2	110.55(13)
O4-C28	1.2672(18)	N1-Ni1-O1	89.23(5)	C3-C2-N1	109.73(13)
N1-C1	1.315(2)	N1-Ni1-O3 ¹	89.89(4)	C2-C3-N2	106.24(13)
N1-C2	1.383(2)	N1-Ni1-O4 ¹	87.37(4)	C5-C4-N2	119.83(13)
N2-C1	1.3581(19)	N1-Ni1-O5	93.89(5)	C9-C4-N2	120.07(14)
N2-C3	1.384(2)	N1-Ni1-C28 ¹	88.08(5)	C9-C4-C5	120.10(14)
N2-C4	1.4218(19)	N4 ² -Ni1-O1	88.46(5)	O1-C19-C20	116.32(14)
N3-C13	1.4251(19)	N4 ² -Ni1-O3 ¹	91.37(4)	O2-C19-O1	125.20(14)
N3-C16	1.378(2)	N4 ² -Ni1-O4 ¹	89.77(5)	O2-C19-C20	118.43(14)
N3-C18	1.3571(19)	N4 ² -Ni1-O5	89.74(5)	C21-C20-C19	110.43(12)
N4-C17	1.377(2)	N4 ² -Ni1-N1	175.90(5)	C22-C21-C20	119.37(15)
N4-C18	1.3138(19)	C6-C5-C4	119.98(14)	C22-C21-C26	118.99(16)
C2-C3	1.343(2)	C5-C6-C7	121.15(14)	C26-C21-C20	121.60(14)
C4-C5	1.389(2)	C6-C7-C8	117.72(14)	C23-C22-C21	121.77(17)
C4-C9	1.384(2)	C6-C7-C10	120.64(14)	C24-C23-C22	119.25(17)
C5-C6	1.380(2)	C8-C7-C10	121.64(14)	C23-C24-C25	119.44(18)
C6-C7	1.395(2)	C9-C8-C7	121.73(14)	C24-C25-C26	122.34(18)
C7-C8	1.396(2)	C8-C9-C4	119.33(14)	C21-C26-C27	123.28(15)
C7-C10	1.484(2)	C11-C10-C7	121.61(14)	C25-C26-C21	118.20(16)
C8-C9	1.384(2)	C15-C10-C7	120.49(14)	C25-C26-C27	118.52(15)
C10-C11	1.394(2)	C12-C11-C10	121.32(14)	C26-C27-C28	116.08(13)
C10-C15	1.394(2)	C15-C10-C11	117.89(14)	O3-C28-Ni1 ³	61.60(8)
C11-C12	1.383(2)	C11-C12-C13	119.34(14)	O3-C28-O4	121.01(14)
C12-C13	1.388(2)	C12-C13-N3	119.73(14)	O3-C28-C27	122.06(13)
C13-C14	1.387(2)	C14-C13-C12	120.58(14)	O4-C28-Ni1 ³	59.43(8)
C14-C15	1.380(2)	C15-C14-C13	119.17(14)	O4-C28-C27	116.92(13)
C16-C17	1.347(2)	C14-C15-C10	121.67(14)	C27-C28-Ni1 ³	176.18(11)
C19-C20	1.529(2)	C17-C16-N3	106.37(13)		
C20-C21	1.510(2)	C16-C17-N4	109.59(14)		
C21-C22	1.397(2)	N4-C18-N3	110.69(13)		
C21-C26	1.399(2)	N4 ² -Ni1-C28 ¹	90.99(5)		
C22-C23	1.380(3)	C19-O1-Ni1	124.06(10)		
C23-C24	1.377(3)	C28-O3-Ni1 ³	87.43(9)		
C24-C25	1.384(3)	C28-O4-Ni1 ³	89.47(9)		
C25-C26	1.387(2)	C1-N1-Ni1	125.28(10)		
C26-C27	1.510(2)	C1-N1-C2	106.35(13)		
C27-C28	1.512(2)	C2-N1-Ni1	126.33(10)		
¹ 2-X,1/2+Y,3/2-Z; ² 2+X,3/2-Y,1/2+Z		¹ 3-X,1/2+Y,3/2-Z; ² 2+X,3/2-Y,1/2+Z; ³ 2-X,-1/2+Y,3/2-Z; ⁴ -2+X,3/2-Y,-1/2+Z			

TableS4. Bond lengths [\AA] and angles [$^\circ$] for $\text{Ni}_{0.6}\text{Co}_{0.4}\text{-MOF}$.

Atom-Atom Length/ \AA	Atom-Atom-Atom	Angle/ $^\circ$	Atom-Atom-Atom	Angle/ $^\circ$	
Co1-O1	2.140(10)	O1-Co1-C28 ¹	132.3(5)	O1-Ni1-O3 ¹	164.0(3)
Co1-O3 ¹	2.132(10)	O3 ¹ -Co1-O1	163.5(5)	O1-Ni1-O4 ¹	103.2(3)
Co1-O4 ¹	2.109(10)	O3 ¹ -Co1-C28 ¹	31.24(15)	O1-Ni1-O5	96.9(3)
Co1-O5	2.093(10)	O4 ¹ -Co1-O1	101.0(4)	O1-Ni1-N1	91.0(3)
Co1-N1	2.107(10)	O4 ¹ -Co1-O3 ¹	62.5(3)	O1-Ni1-N4 ²	88.5(2)
Co1-N4 ²	2.065(10)	O4 ¹ -Co1-C28	31.30(15)	O1-Ni1-C28 ¹	133.6(3)
Co1-C28 ¹	2.436(10)	O5-Co1-O1	94.4(4)	O3 ¹ -Ni1-C28 ¹	30.35(9)
O1-C19	1.2748(18)	O5-Co1-O3 ¹	102.1(4)	O4 ¹ -Ni1-O3 ¹	60.77(17)
O1-Ni1	2.051(6)	O5-Co1-O4 ¹	164.6(5)	O4 ¹ -Ni1-C28 ¹	30.42(9)
O2-C19	1.2471(19)	O5-Co1-N1	93.2(4)	O5-Ni1-O3 ¹	99.1(3)
O3-C28	1.2646(18)	O5-Co1-C28 ¹	133.3(5)	O5-Ni1-O4 ¹	159.7(3)
O4-C28	1.2660(18)	N1-Co1-O1	87.6(4)	O5-Ni1-C28 ¹	129.4(3)
O5-Ni1	2.099(6)	N1-Co1-O3 ¹	90.3(4)	N1-Ni1-O3 ¹	88.8(2)
N1-C1	1.3805(19)	N1-Co1-O4 ¹	87.7(4)	N1-Ni1-O4 ¹	88.0(2)
N1-C3	1.3201(18)	N1-Co1-C28 ¹	88.7(4)	N1-Ni1-O5	94.1(3)
N1-Ni1	2.072(6)	N4 ² -Co1-O1	87.0(4)	N1-Ni1-N4 ²	176.3(4)
N2-C2	1.3821(19)	N4 ² -Co1-O3 ¹	93.9(4)	N1-Ni1-C28 ¹	87.8(2)
N2-C3	1.3605(18)	N4 ² -Co1-O4 ¹	89.9(4)	N4 ² -Ni1-O3 ¹	90.6(2)
N2-C4	1.4289(17)	N4 ² -Co1-O5	90.6(4)	N4 ² -Ni1-O4 ¹	88.5(2)
N3-C13	1.4313(17)	N4 ² -Co1-N1	173.6(6)	N4 ² -Ni1-O5	89.7(2)
N3-C16	1.3639(17)	N4 ² -Co1-C28 ¹	92.4(4)	N4 ² -Ni1-C28 ¹	89.9(2)
N3-C17	1.378(2)	C19-O1-Co1	124.4(3)	C9-C4-C5	120.06(13)
N4-C16	1.3209(18)	C19-O1-Ni1	124.2(2)	C4-C5-C6	119.44(14)
N4-C18	1.3778(19)	C28-O3-Co1 ³	87.8(3)	C5-C6-C7	121.56(13)
C1-C2	1.3586(19)	C28-O4-Co1 ³	88.7(3)	C6-C7-C8	117.80(13)
C4-C5	1.3906(19)	C1-N1-Co1	127.5(3)	C6-C7-C10	121.41(13)
C4-C9	1.390(2)	C1-N1-Ni1	125.4(2)	C8-C7-C10	120.78(13)
C5-C6	1.394(2)	C3-N1-Co1	123.9(3)	C9-C8-C7	121.25(14)
C6-C7	1.397(2)	C3-N1-C1	106.28(12)	C8-C9-C4	119.89(13)
C7-C8	1.3990(19)	C3-N1-Ni1	126.3(2)	C11-C10-C7	120.63(14)
C7-C10	1.4904(19)	C2-N2-C4	127.04(12)	C15-C10-C7	121.56(13)
C8-C9	1.3899(19)	C3-N2-C2	107.16(12)	C15-C10-C11	117.80(13)
C10-C11	1.397(2)	C3-N2-C4	125.73(13)	C12-C11-C10	121.63(14)
C10-C15	1.393(2)	C16-N3-C13	125.86(12)	C13-C12-C11	119.33(13)
C11-C12	1.3924(19)	C16-N3-C17	107.10(11)	C12-C13-N3	119.72(13)
C12-C13	1.383(2)	C17-N3-C13	127.03(12)	C12-C13-C14	120.41(13)
C13-C14	1.393(2)	C16-N4-Co1 ⁴	127.1(3)	C14-C13-N3	119.87(13)
C14-C15	1.3930(19)	C16-N4-C18	106.27(12)	C13-C14-C15	119.46(14)
C17-C18	1.3608(19)	C18-N4-Co1 ⁴	126.6(3)	C14-C15-C10	121.34(13)
C19-C20	1.530(2)	C2-C1-N1	109.63(13)	N4-C16-N3	110.74(13)
C20-C21	1.515(2)	C1-C2-N2	106.13(13)	C18-C17-N3	106.24(13)
C21-C22	1.394(2)	N1-C3-N2	110.80(13)	C17-C18-N4	109.64(13)
C21-C26	1.406(2)	C5-C4-N2	120.20(13)	O1-C19-C20	116.48(14)
C22-C23	1.383(3)	C9-C4-N2	119.74(12)	O2-C19-O1	125.23(14)
¹ X,1/2+Y,3/2-Z; ² - 2+X,3/2-Y,1/2+Z		¹ -X,1/2+Y,3/2-Z; ² -2+X,3/2-Y,1/2+Z; ³ -X,-1/2+Y,3/2-Z; ⁴ 2+X,3/2-Y,- 1/2+Z			

Table S5 ICP-MS chart of Ni_{0.6}Co_{0.4}-MOF.

Sample mass (g)	Test element	Element concentration (mg/L)	Content
0.0024	Co	10.66	4.4422%
0.0024	Ni	14.43	6.0133%

TableS6. H-Bond lengths [\AA] and angles [$^\circ$] for Ni-MOF (1) and Ni_{0.6}Co_{0.4}-MOF (2).

1: Donor --- H....Acceptor	D - H	H...A	D...A	D - H...A
O5---H5A....O2	0.85	1.85	2.6049(15)	147
O5---H5B....O1	0.85	2.08	2.8847(15)	159
C1---H1....O4	0.93	2.22	3.1400(19)	169
C6---H6....O2	0.93	2.37	3.2432(19)	157
C14---H14....O3	0.93	2.43	3.3564(18)	179
C18---H18....O4	0.93	2.55	3.0292(18)	112
C27---H27B....O2	0.97	2.43	3.283(2)	146
2: Donor --- H....Acceptor	D - H	H...A	D...A	D - H...A
O5---H5A....O2	0.88	1.83	2.6078(15)	146
O5---H5B....O1	0.83	2.16	2.8979(14)	149
C3---H3....O4	0.95	2.21	3.1434(19)	169
C8---H8....O2	0.95	2.35	3.2434(19)	156
C12---H12....O3	0.95	2.41	3.3621(18)	179
C16---H16....O4	0.95	2.57	3.0471(18)	112
C27---H27A....O2	0.99	2.42	3.290(2)	147

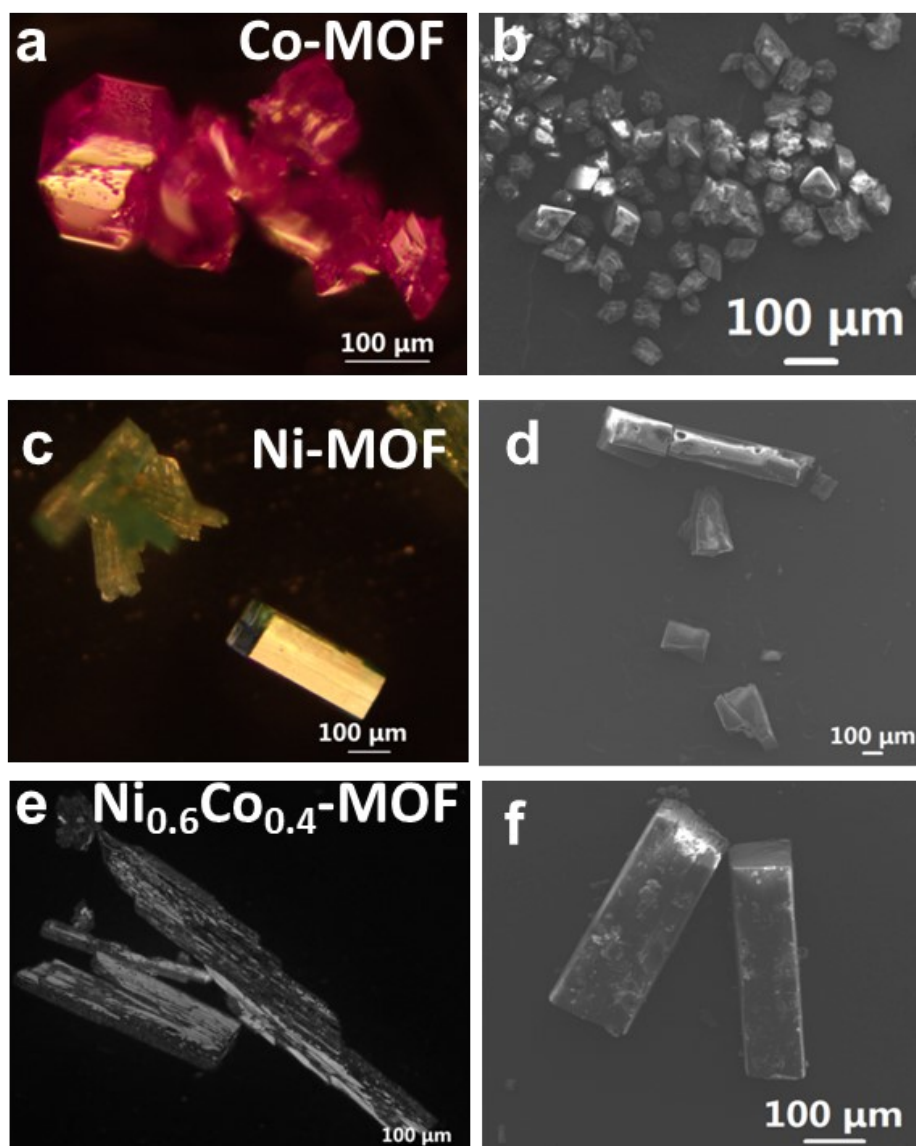


Fig. S5 (a) The optical image under the metallographic microscope and (b) SEM of Co-MOF; (c) The optical image under the metallographic microscope and (d) SEM of Ni-MOF; (e) The optical image under the metallographic microscope and (f) SEM of Ni_{0.6}Co_{0.4}-MOF. Specifically, the colour of the crystals in the metallurgical microscope is adjusted by means of a colorimetric plate in the instrument's own program, in order to facilitate a better return of the raw material's own unique colour.

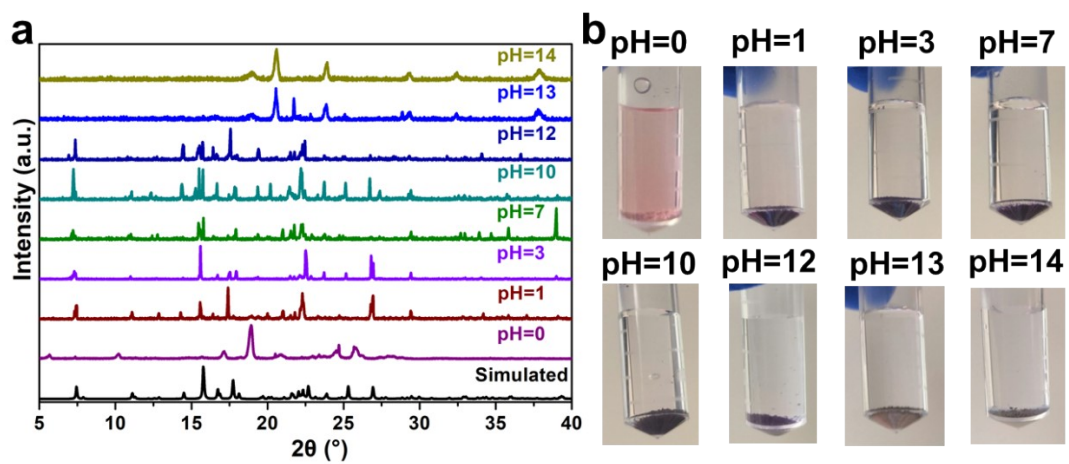


Fig. S6 (a) p-XRD of Co-MOF incubated at different pH for 24 hours; (b) Optical images of Co-MOF corresponding to incubation at different pH for 24 hours.

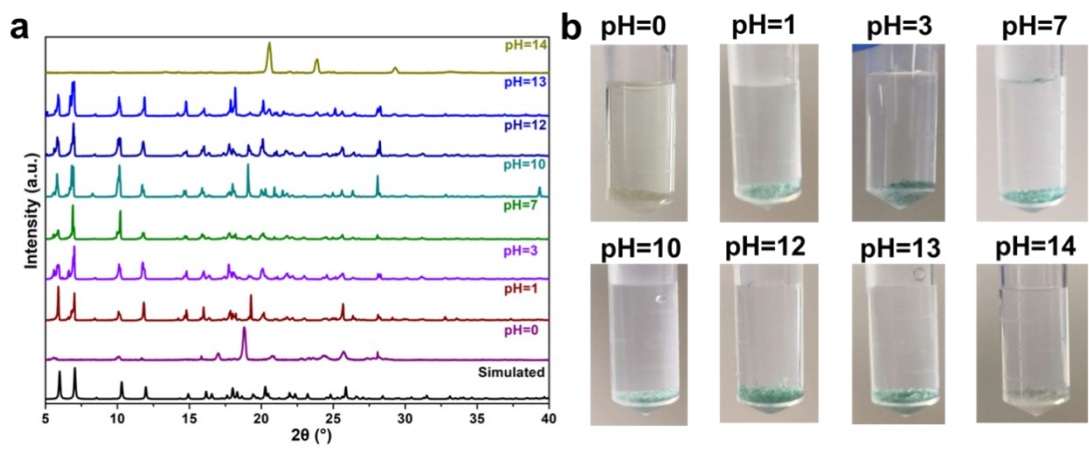


Fig. S7 (a) p-XRD of Ni-MOF incubated at different pH for 24 hours; (b) Optical images of Ni-MOF corresponding to incubation at different pH for 24 hours.

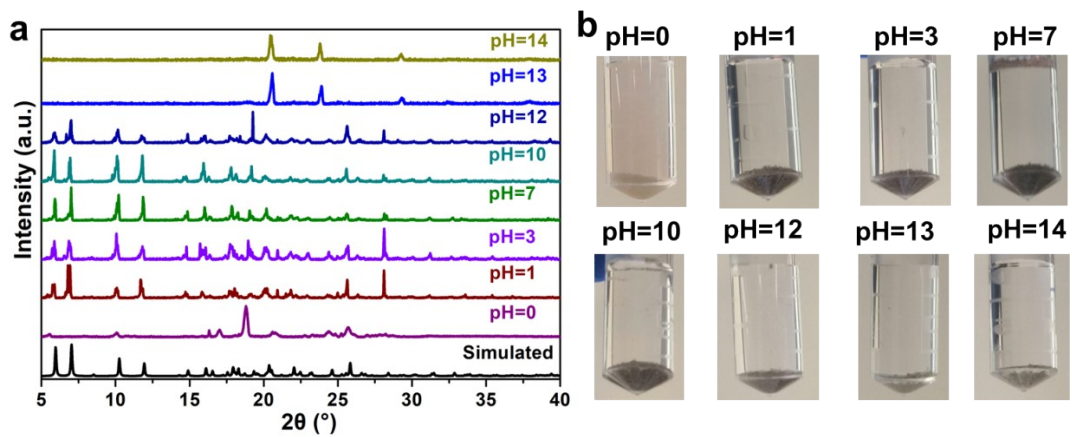


Fig. S8 (a) XRD of $\text{Ni}_{0.6}\text{Co}_{0.4}\text{-MOF}$ incubated at different pH for 24 hours; (b) Optical images corresponding to $\text{Ni}_{0.6}\text{Co}_{0.4}\text{-MOF}$ incubated at different pH for 24 hours.

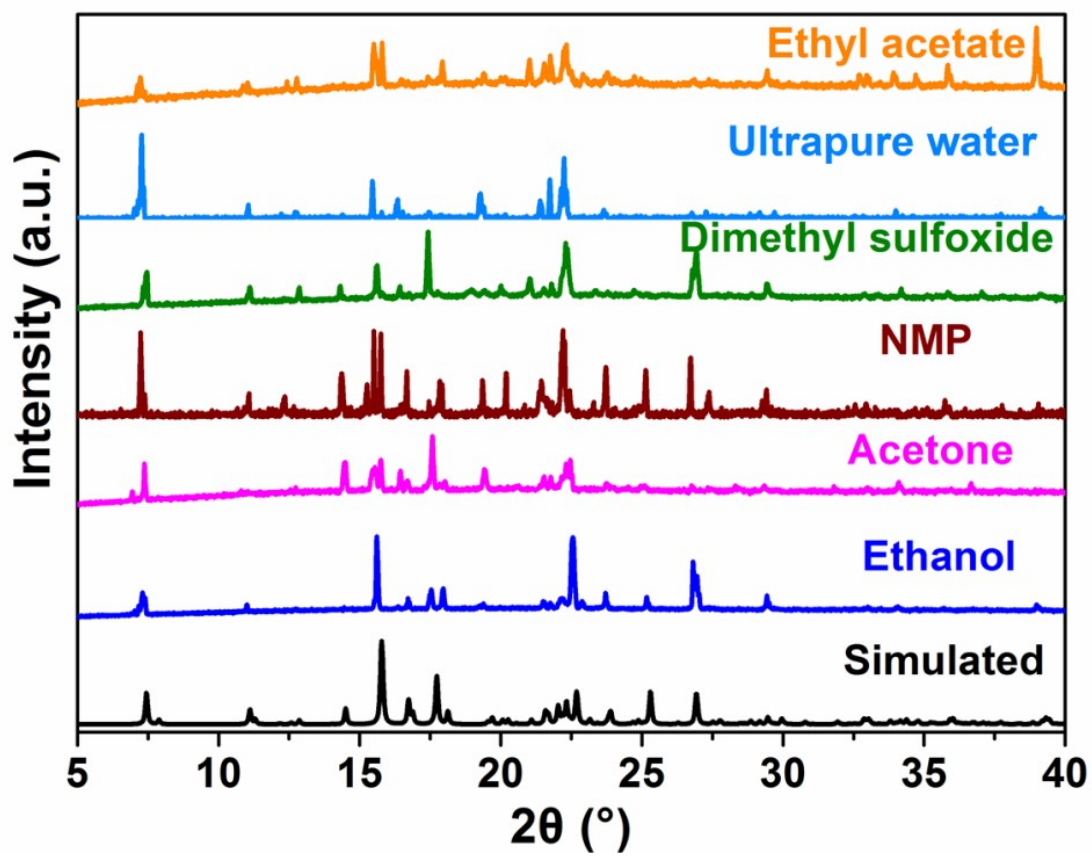


Fig. S9 XRD pattern of Co-MOF stored in different solvents for 7 days.

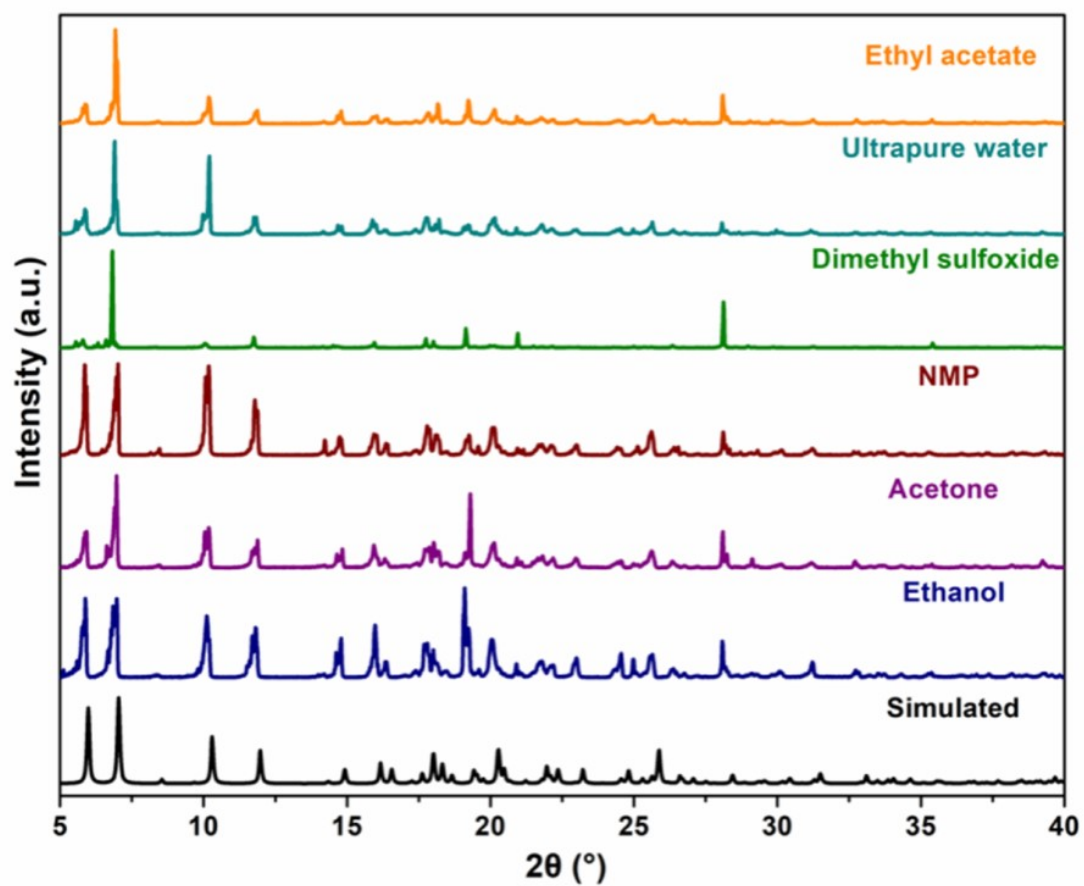


Fig. S10 XRD pattern of Ni-MOF stored in different solvents for 7 days.

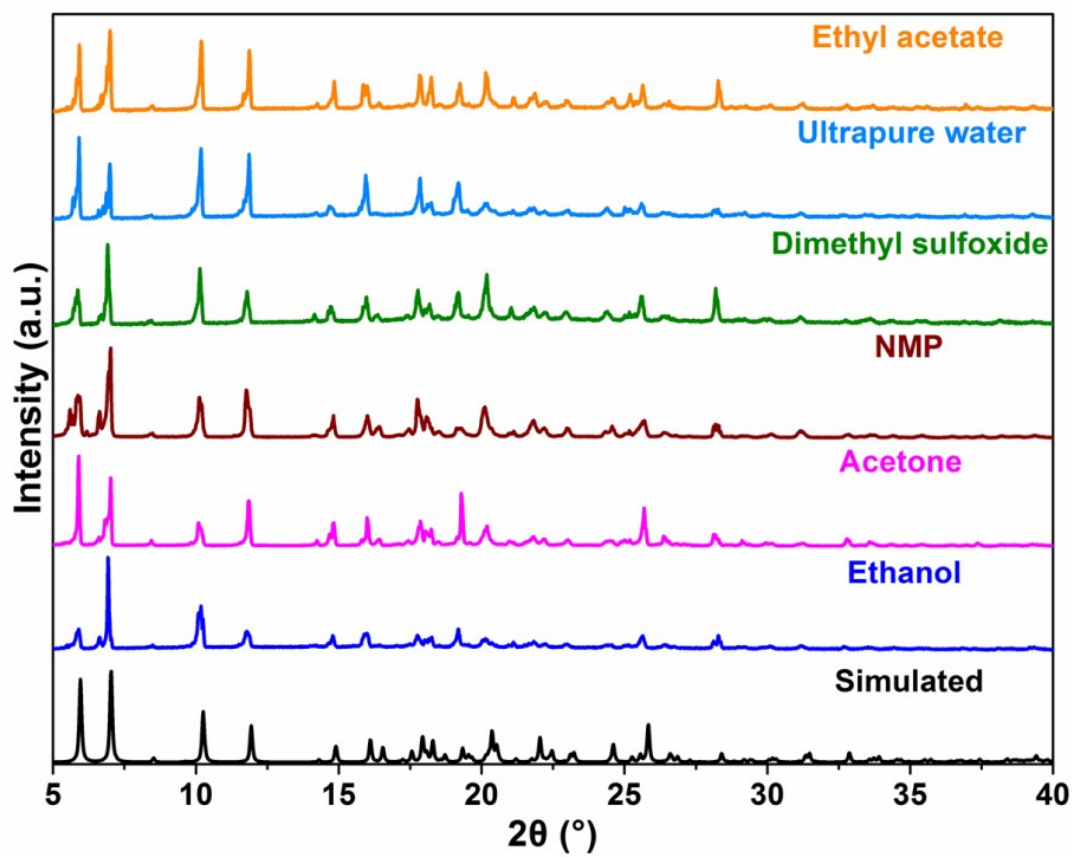


Fig. S11 XRD pattern of $\text{Ni}_{0.6}\text{Co}_{0.4}\text{-MOF}$ stored in different solvents for 7 days.

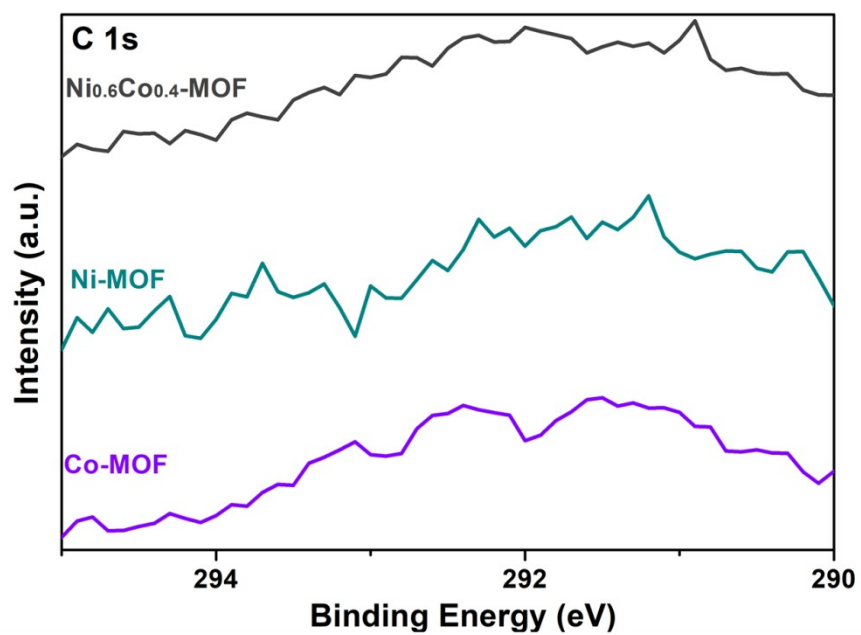


Fig. S12 Local fine spectra (π - π action) of C1s for Co-MOF, Ni-MOF, and Ni_{0.6}Co_{0.4}-MOF.

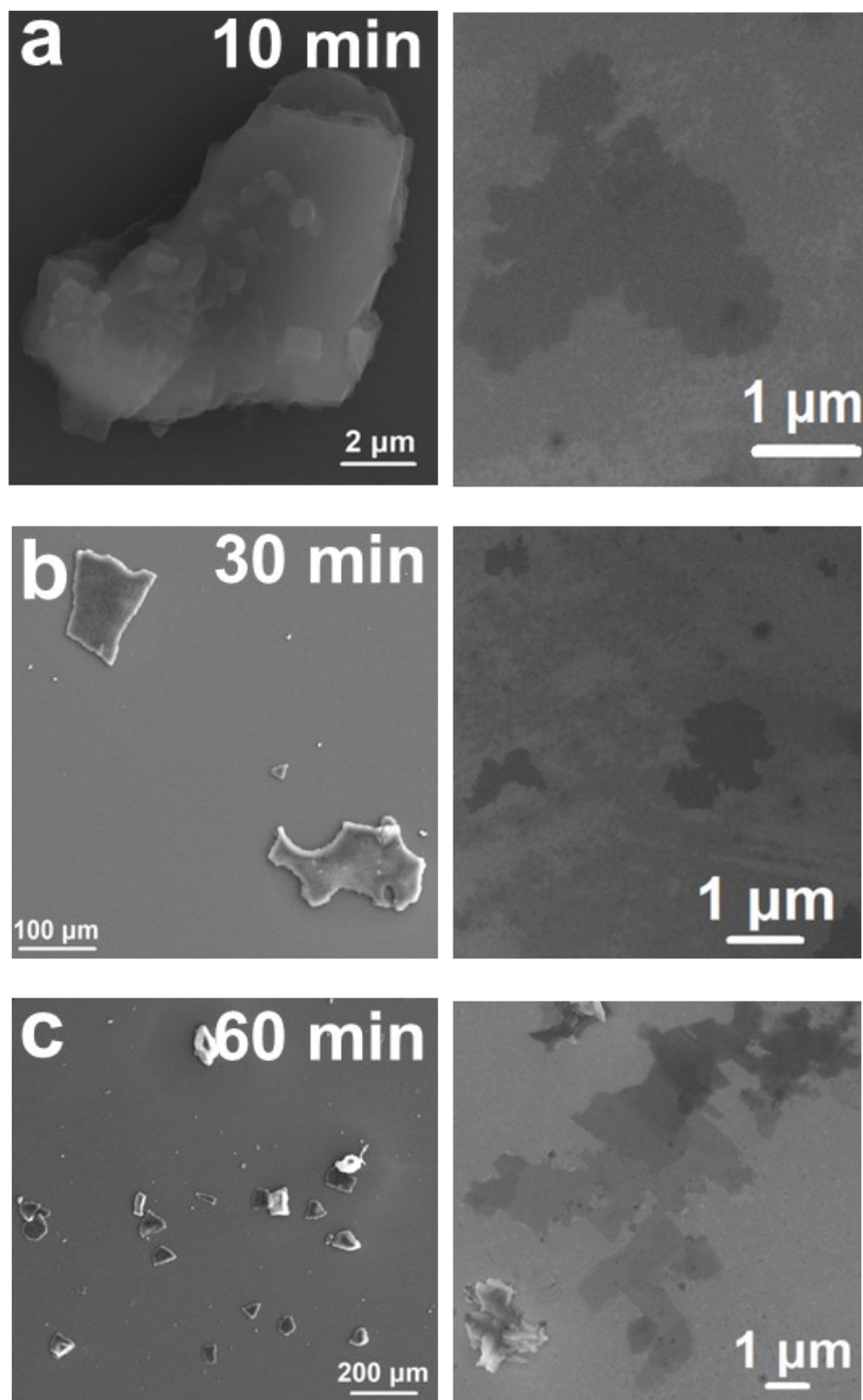


Fig. S13 SEM of $\text{Ni}_{0.6}\text{Co}_{0.4}\text{-MOF}$ was obtained by exfoliating at 60W for different reaction times (a-c: 10 min, 30 min and 60 min). Left: The main morphology of $\text{Ni}_{0.6}\text{Co}_{0.4}\text{-MOF}$ after exfoliation. Right: A small number of $\text{Ni}_{0.6}\text{Co}_{0.4}\text{-MOF}$ nanosheets are generated at this power.

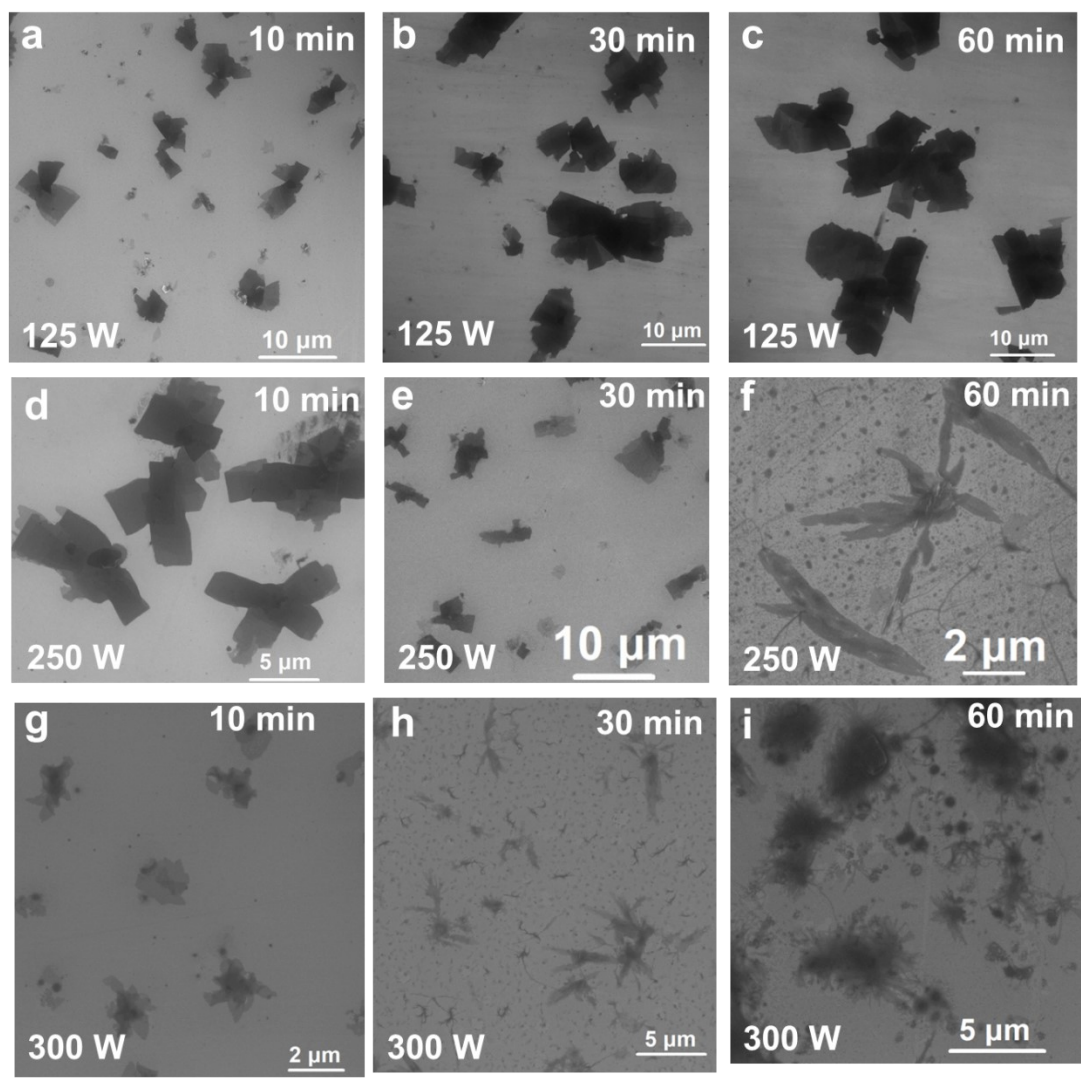


Fig. S14 SEM of $\text{Ni}_{0.6}\text{Co}_{0.4}$ -MOF nanosheet was obtained by exfoliating at 125 W for 10 min (a), 30 min (b) and 60 min (c); SEM of $\text{Ni}_{0.6}\text{Co}_{0.4}$ -MOF nanosheet was obtained by exfoliating at 250 W for 10 min (d), 30 min (e) and 60 min (f); SEM of $\text{Ni}_{0.6}\text{Co}_{0.4}$ -MOF nanosheet was obtained by exfoliating at 300 W for 10 min (g), 30 min (h) and 60 min (i).

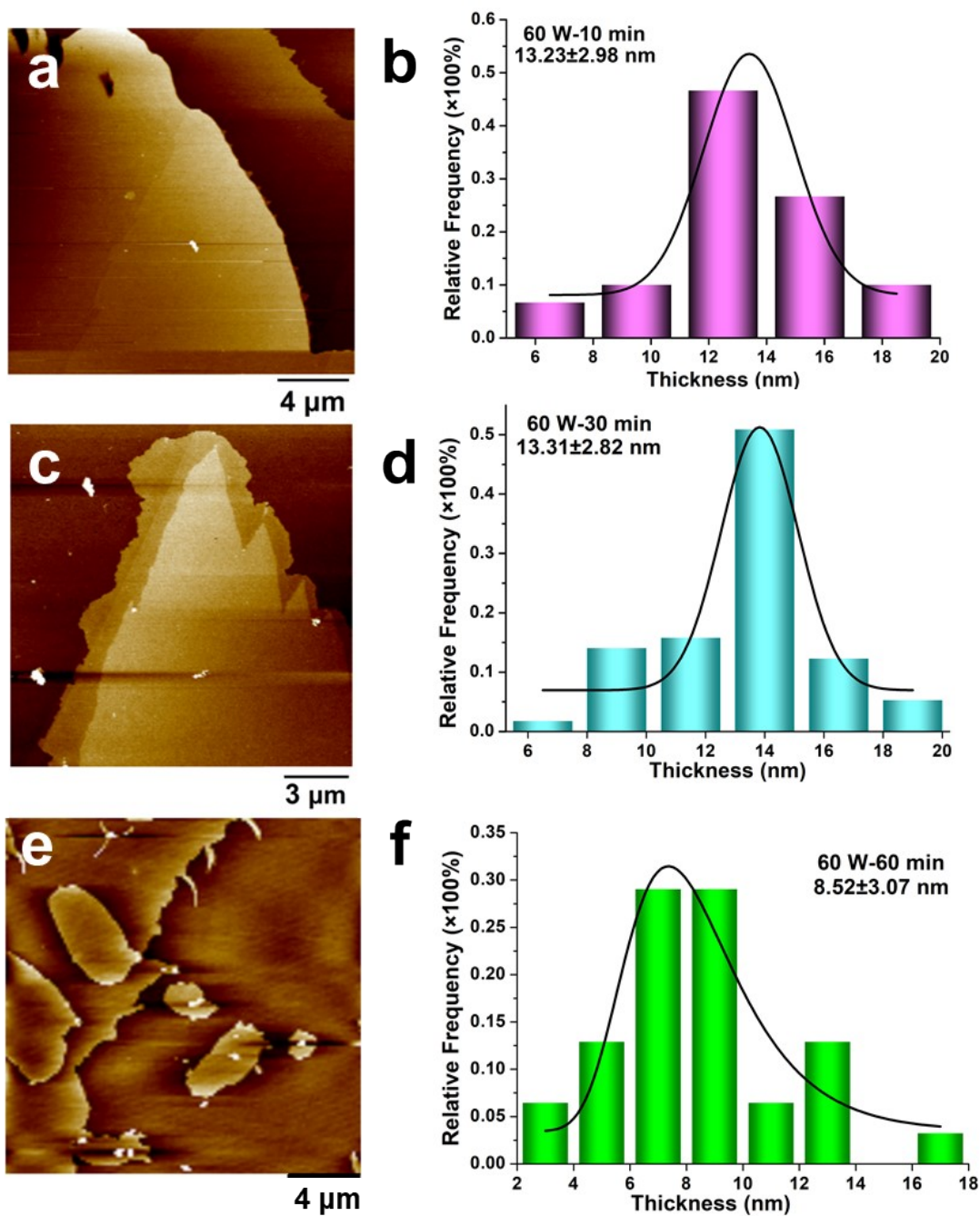
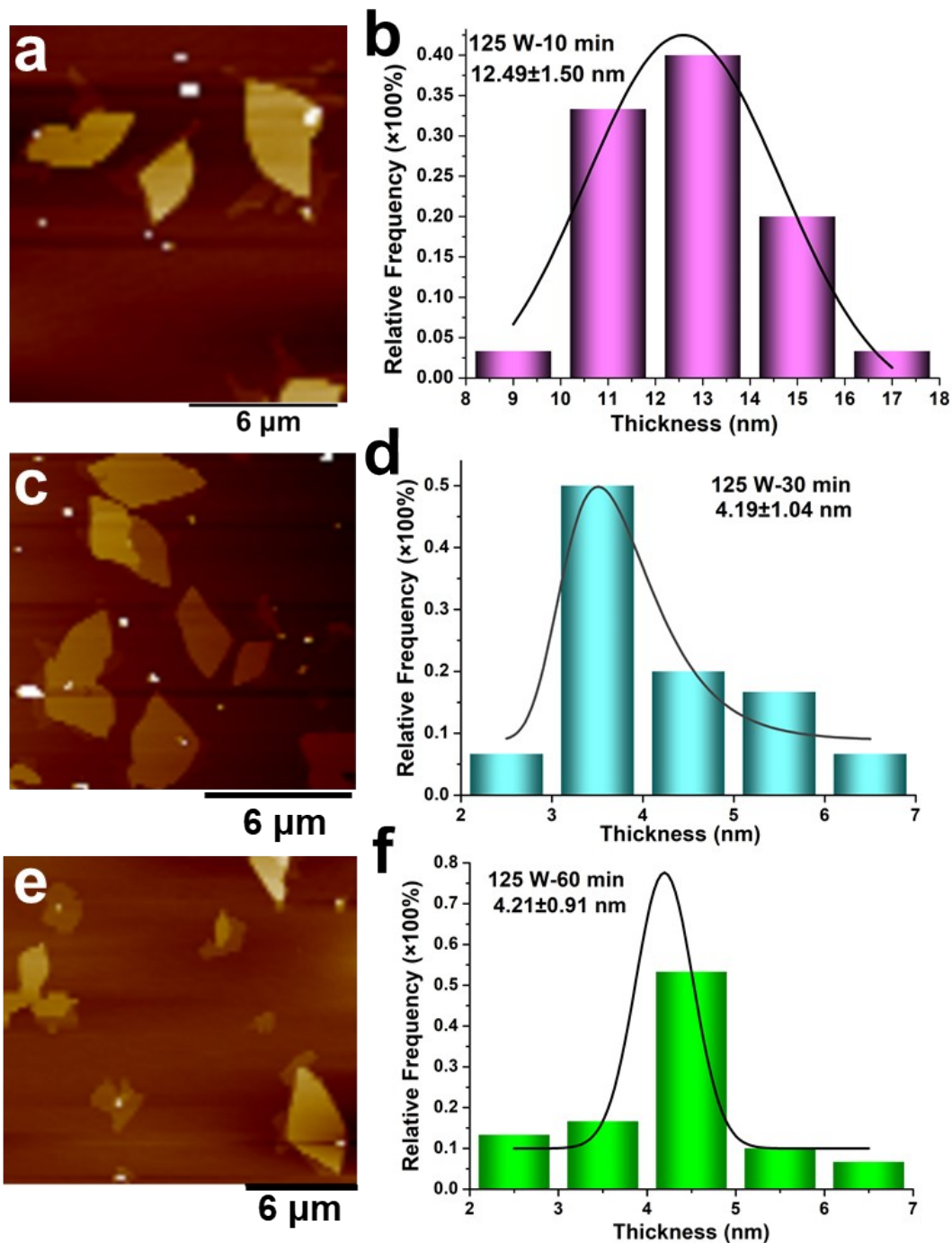


Fig. S15 (a) AFM of $\text{Ni}_{0.6}\text{Co}_{0.4}\text{-MOF}$ nanosheet was obtained by exfoliating at 60 W for 10 min; (b) The thickness statistics of the corresponding nanosheets in Figure S15a; (c) AFM of $\text{Ni}_{0.6}\text{Co}_{0.4}\text{-MOF}$ nanosheet was obtained by exfoliating at 60 W for 30 min; (d) The thickness statistics of the corresponding nanosheets in Figure S15c; (e) AFM of $\text{Ni}_{0.6}\text{Co}_{0.4}\text{-MOF}$ nanosheet was obtained by exfoliating at 60 W for 60 min; (f) The thickness statistics of the corresponding nanosheets in Figure S15e.



F

ig. S16 (a) AFM of $\text{Ni}_{0.6}\text{Co}_{0.4}$ -MOF nanosheet was obtained by exfoliating at 125 W for 10 min; (b) The thickness statistics of the corresponding nanosheets in Figure S16a; (c) AFM of $\text{Ni}_{0.6}\text{Co}_{0.4}$ -MOF nanosheet was obtained by exfoliating at 125 W for 30 min; (d) The thickness statistics of the corresponding nanosheets in Figure S16c; (e) AFM of $\text{Ni}_{0.6}\text{Co}_{0.4}$ -MOF nanosheet was obtained by exfoliating at 125 W for 60 min; (f) The thickness statistics of the corresponding nanosheets in Figure S16e.

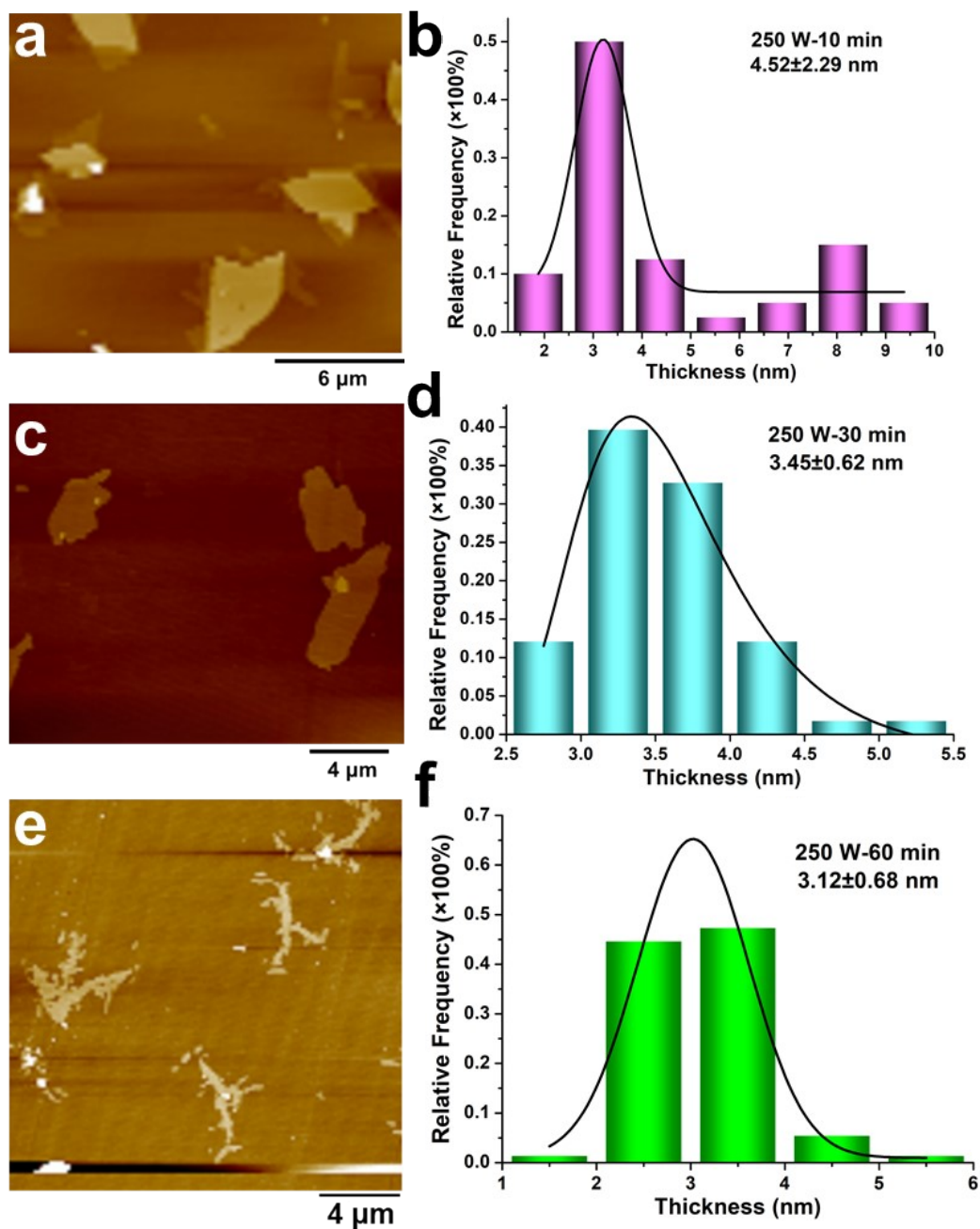


Fig. S17 (a) AFM of $\text{Ni}_{0.6}\text{Co}_{0.4}\text{-MOF}$ nanosheet was obtained by exfoliating at 250 W for 10 min; (b) The thickness statistics of the corresponding nanosheets in Figure S17a; (c) AFM of $\text{Ni}_{0.6}\text{Co}_{0.4}\text{-MOF}$ nanosheet was obtained by exfoliating at 250 W for 30 min; (d) The thickness statistics of the corresponding nanosheets in Figure S17c; (e) AFM of $\text{Ni}_{0.6}\text{Co}_{0.4}\text{-MOF}$ nanosheet was obtained by exfoliating at 250 W for 60 min; (f) The thickness statistics of the corresponding nanosheets in Figure S17e.

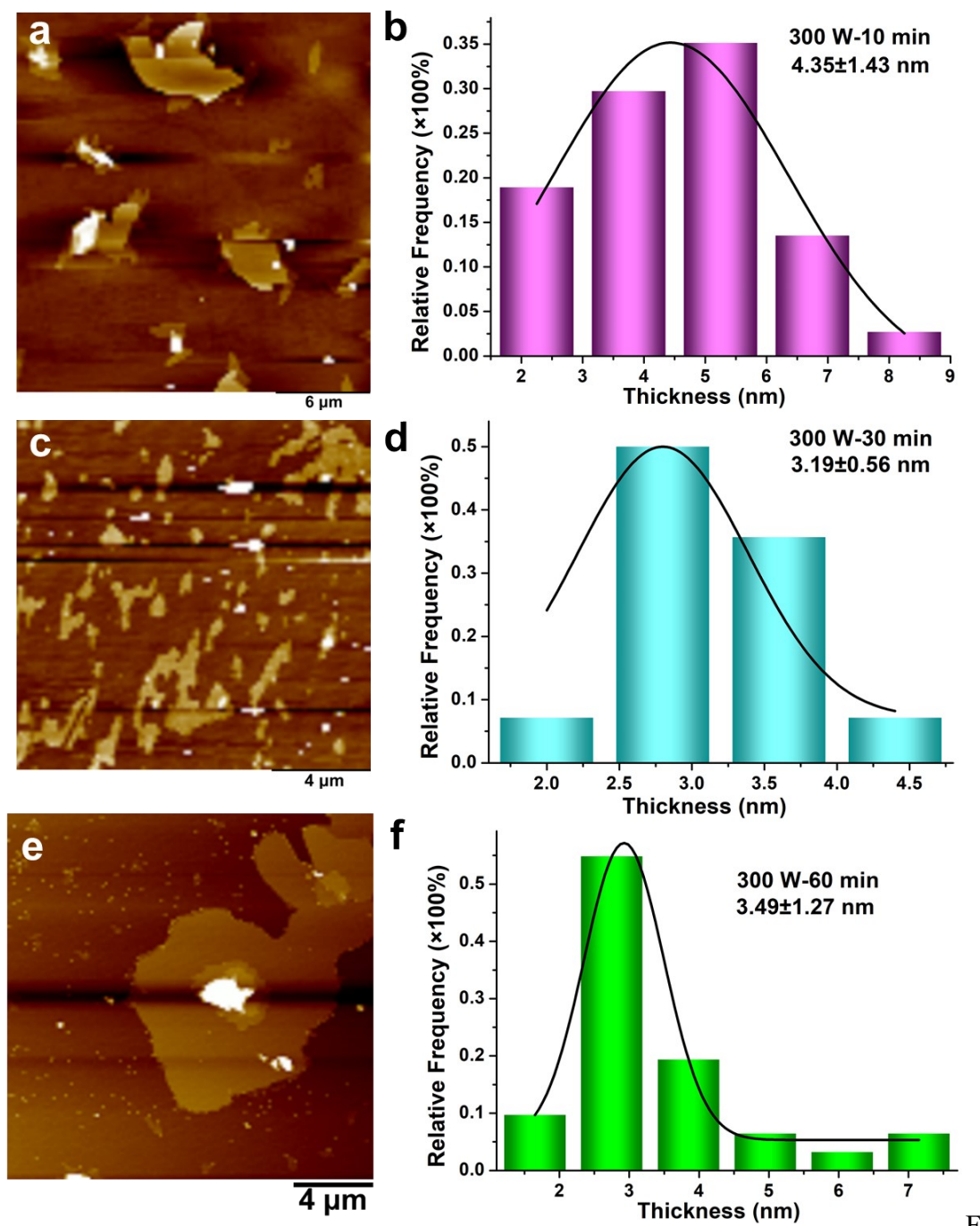


Fig. S18 (a) AFM of $\text{Ni}_{0.6}\text{Co}_{0.4}\text{-MOF}$ nanosheet was obtained by exfoliating at 300 W for 10 min; (b) The thickness statistics of the corresponding nanosheets in Figure S18a; (c) AFM of $\text{Ni}_{0.6}\text{Co}_{0.4}\text{-MOF}$ nanosheet was obtained by exfoliating at 300 W for 30 min; (d) The thickness statistics of the corresponding nanosheets in Figure S18c; (e) AFM of $\text{Ni}_{0.6}\text{Co}_{0.4}\text{-MOF}$ nanosheet was obtained by exfoliating at 300 W for 60 min; (f) The thickness statistics of the corresponding nanosheets in Figure S18e.

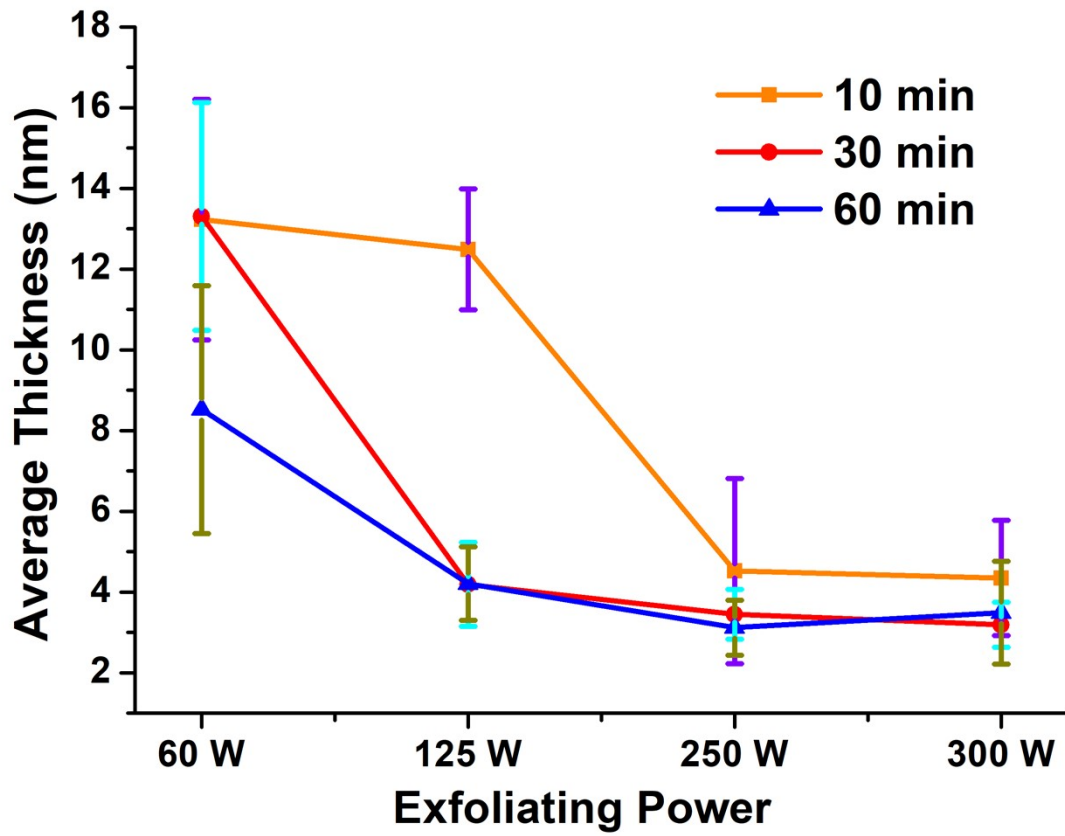


Fig. S19 Dependence of average thickness on exfoliation power.

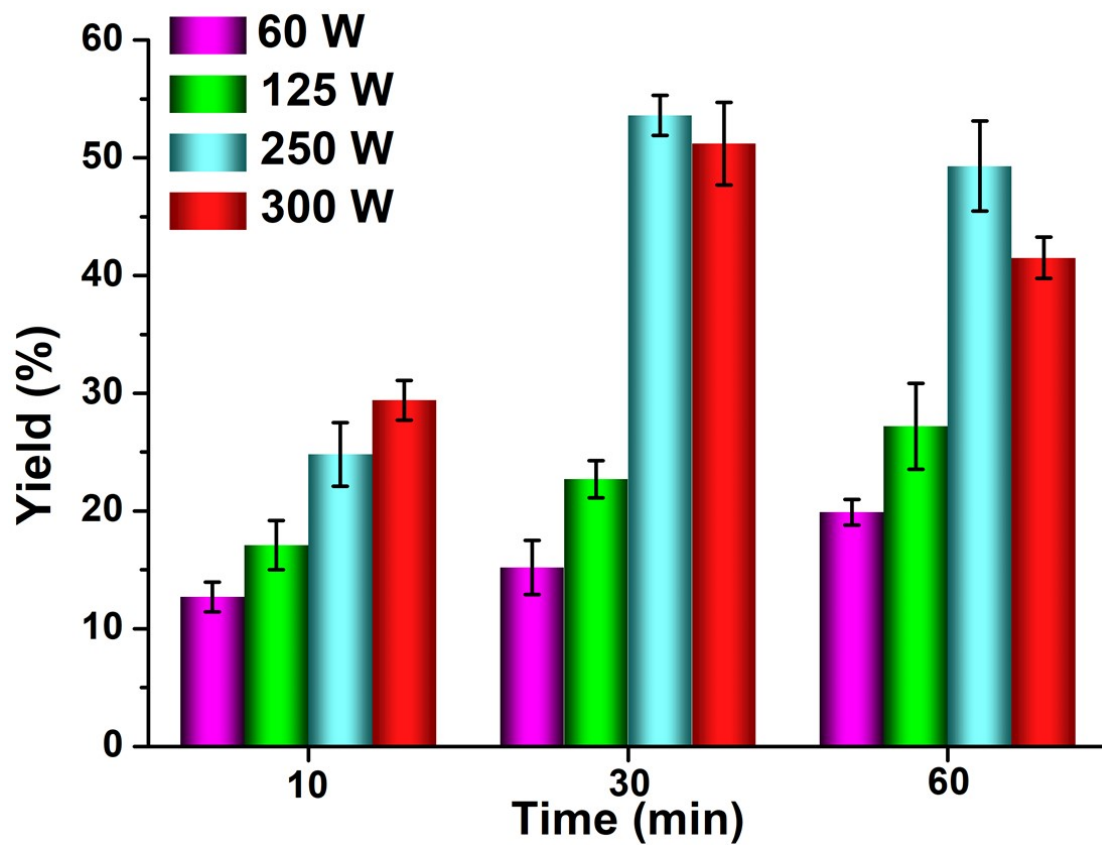


Fig. S20 Yield statistics of nanosheets obtained under different exfoliation parameters, (mass percentage).

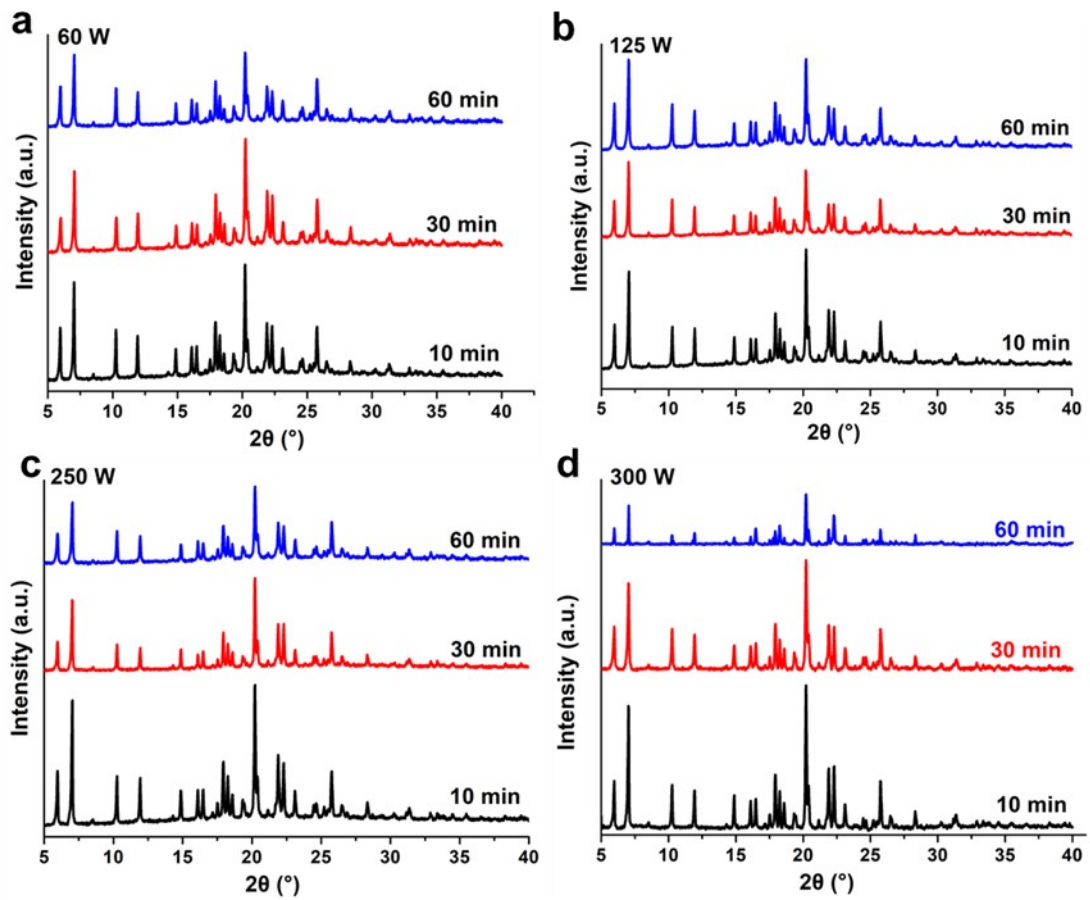


Fig. S21 (a) XRD of $\text{Ni}_{0.6}\text{Co}_{0.4}\text{-MOF NHs}$ was obtained by exfoliating at 60 W for 10 min, 30 min and 60 min; (b) XRD of $\text{Ni}_{0.6}\text{Co}_{0.4}\text{-MOF NHs}$ was obtained by exfoliating at 125 W for 10 min, 30 min and 60 min; (c) XRD of $\text{Ni}_{0.6}\text{Co}_{0.4}\text{-MOF NHs}$ was obtained by exfoliating at 250 W for 10 min, 30 min and 60 min; (d) XRD of $\text{Ni}_{0.6}\text{Co}_{0.4}\text{-MOF NHs}$ was obtained by exfoliating at 300 W for 10 min, 30 min and 60 min.

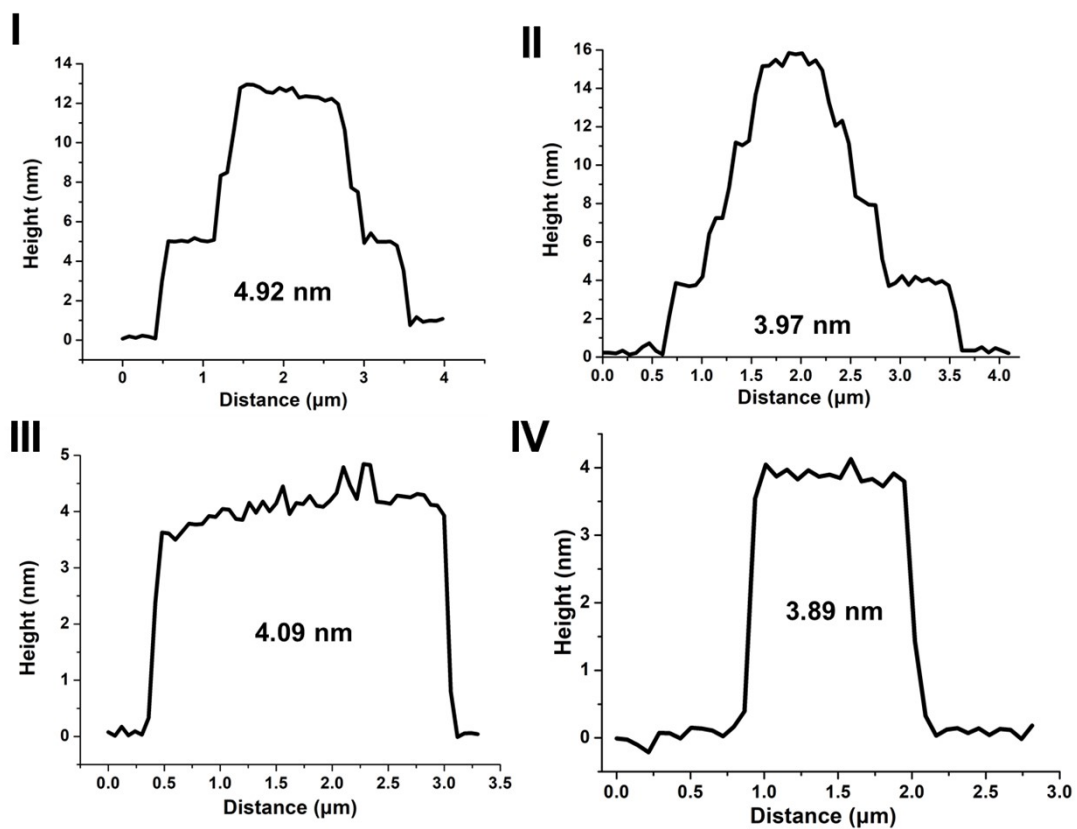


Fig. S22 AFM measurement of Ni_{0.6}Co_{0.4}-MOF NHs height statistics, where I and II only count the height of the last layer.

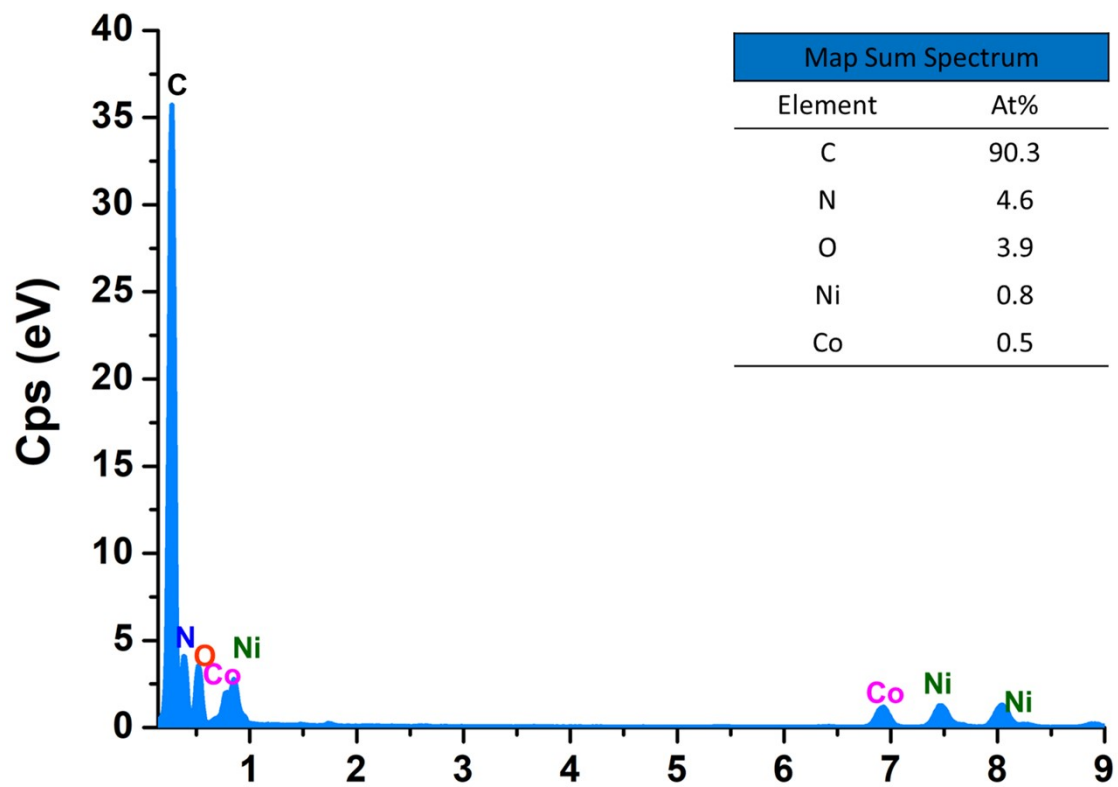


Fig. S23 The Map Sum Spectrum of Ni_{0.6}Co_{0.4}-MOF NHs.

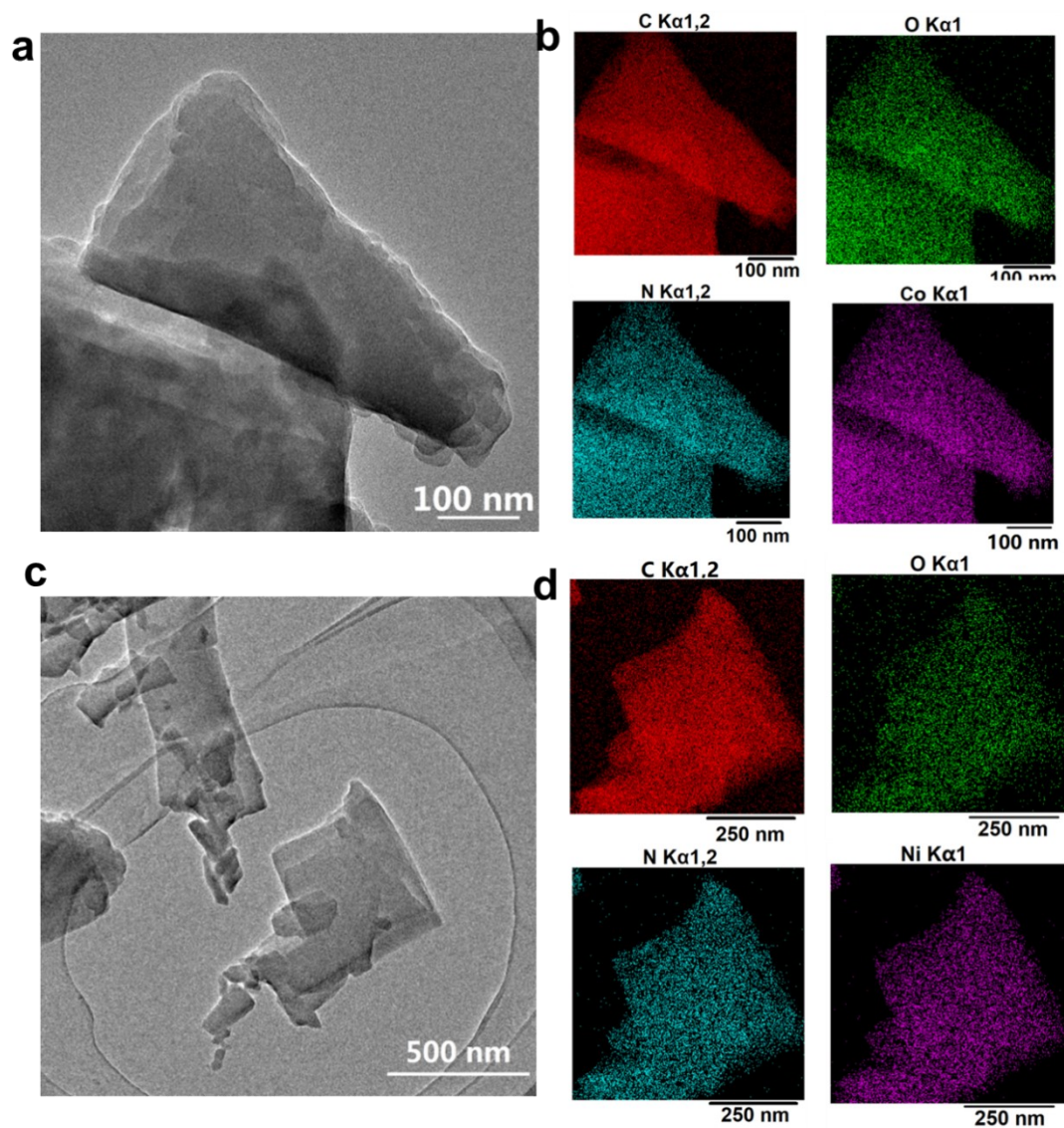


Fig. S24 (a) TEM of Co-MOF NHs (250 W, 30 min); (b) and corresponding elemental mapping; (c) TEM of Ni-MOF NHs (250 W, 30 min); (d) and corresponding elemental mapping.

Table. S7 Parameter comparison of MOF nanosheets prepared by traditional ultrasonic exfoliation and cell fragmentation probe-assisted mode.

MOF	Time (h)	Power (W)	Yield (%)	Average Thickness (nm)	References
Cu(n)(DMF)	12	350-380	-	20±12—35±26	S2
HNU-68-N	1	-	8	4.4	S3
2,3-MTV-MONs	12	320	-	12±6	S4
Cd-MOF/Tb ³⁺	6	100	-	1.4	S5
nBMOF	24-96	-	-	2.5	S6
MOF1, MOF2	> 1	-	-	3±0.5	S7
Cu(1)(DMF), Cu(2)(DMF)	0.5-12	320	-	19±9—59±35	S8
[Cu(2,5pydc)(H 2O)] _n ·2H ₂ O	1	550	-	126 ± 35	S9
Zn(Bim)(OAc)	5	300	21	3-4	S10
Ni _{0.6} Co _{0.4} -MOF	0.5	250	53.6	3.45±0.62	This work

Note: The yield and effectiveness of exfoliation is also affected by the interlayer forces of the MOF itself. Stronger interlayer forces may mean that different parameters need to be adjusted and the solvent changed to match the surface energy in order to achieve the desired exfoliation.

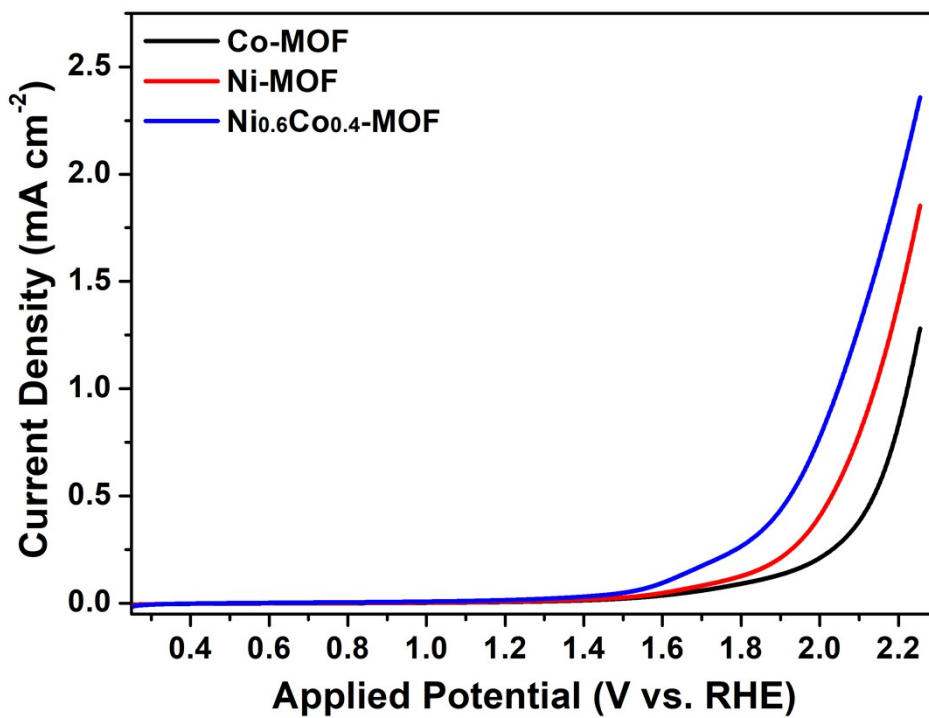


Fig. S25 LSV plot of Co-MOF, Ni-MOF, Ni_{0.6}Co_{0.4}-MOF.

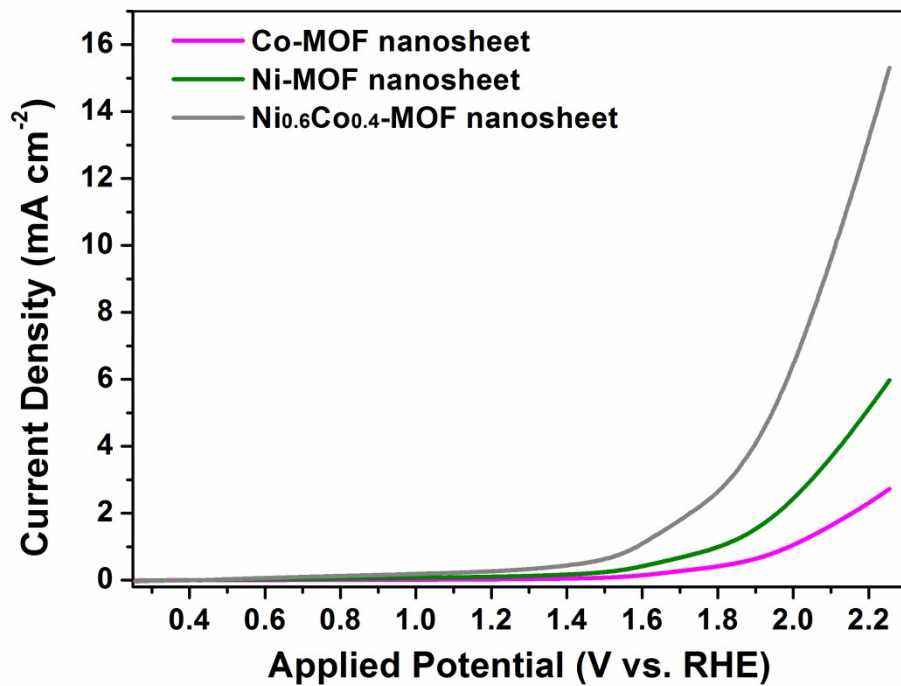


Figure S26 LSV curve of Co-MOF NHs, Ni-MOF NHs and Ni_{0.6}Co_{0.4}-MOF NHs.

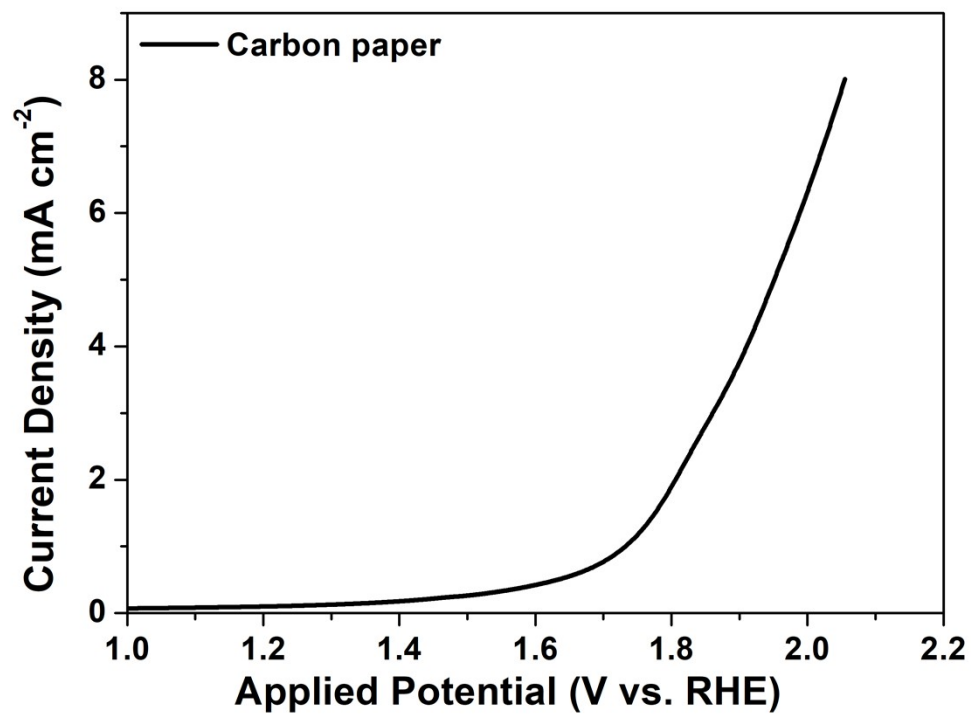


Fig. S27 LSV plot of carbon paper.

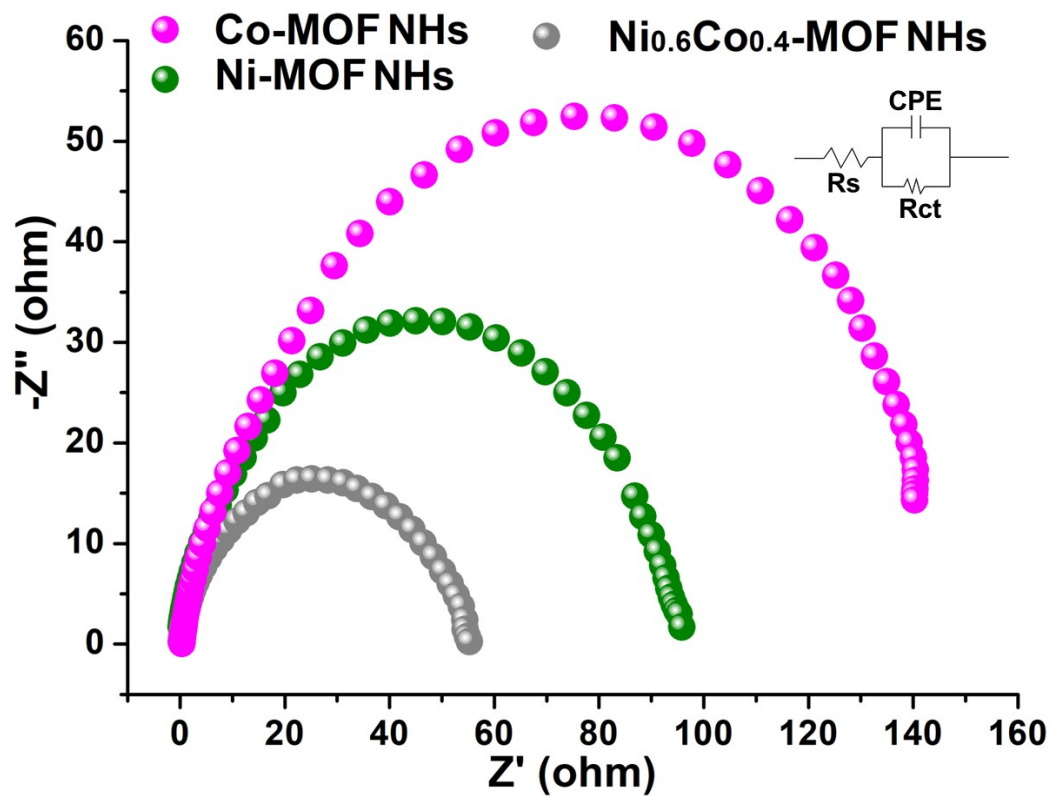


Fig. S28 Nyquist plots of Ni-MOF NHs, Co-MOF NHs, $Ni_{0.6}Co_{0.4}$ -MOF NHs. Insert: Equivalent circuit diagram.

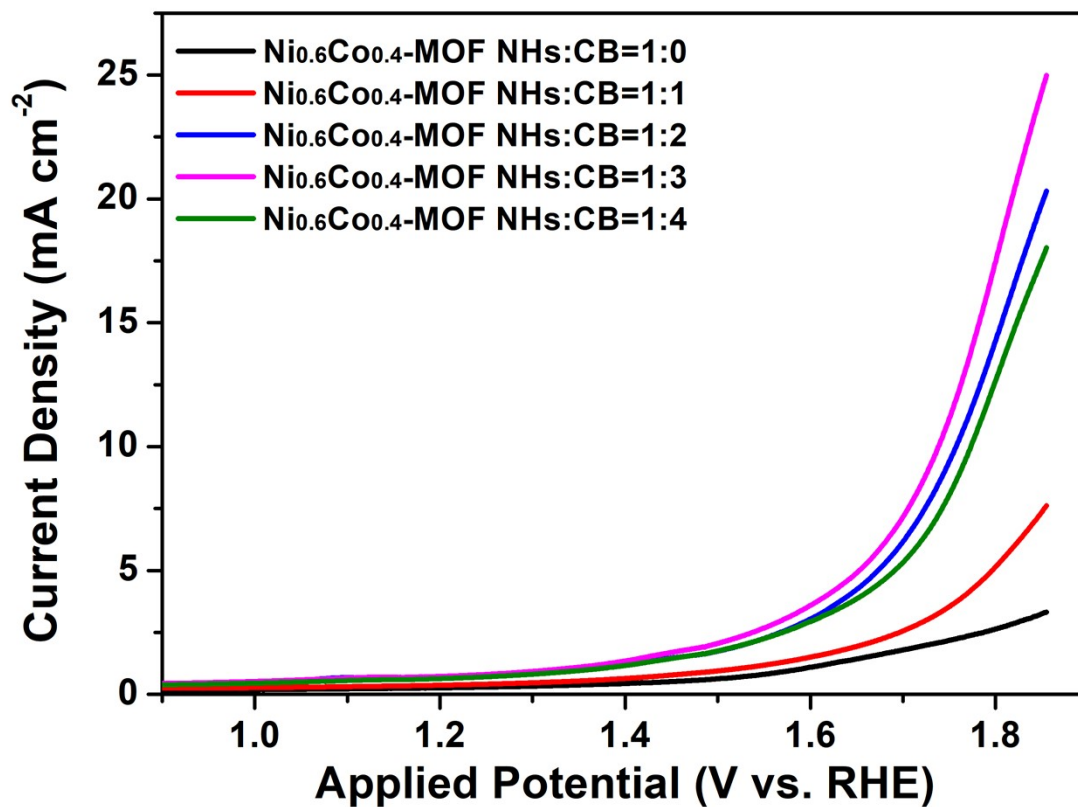


Fig. S29 LSV diagram of the composite ratio of the Ni_{0.6}Co_{0.4}-MOF NHs to CB.

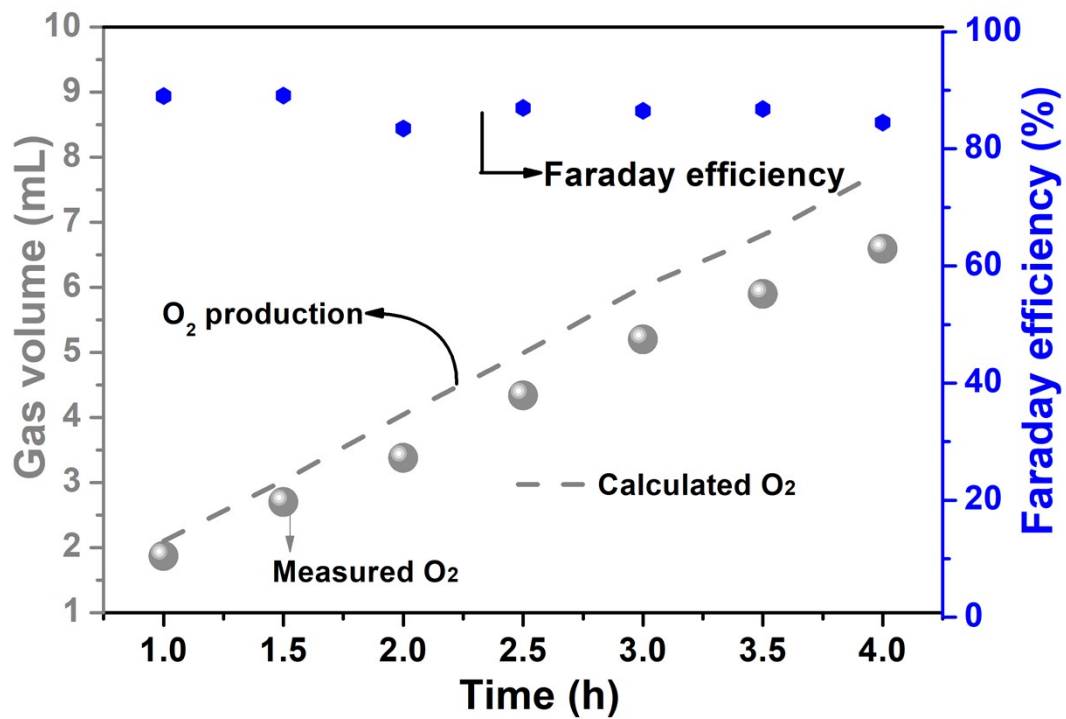


Fig. S30 Faraday efficiency of Ni_{0.6}Co_{0.4}-MOF NHs/CB for O₂ production.

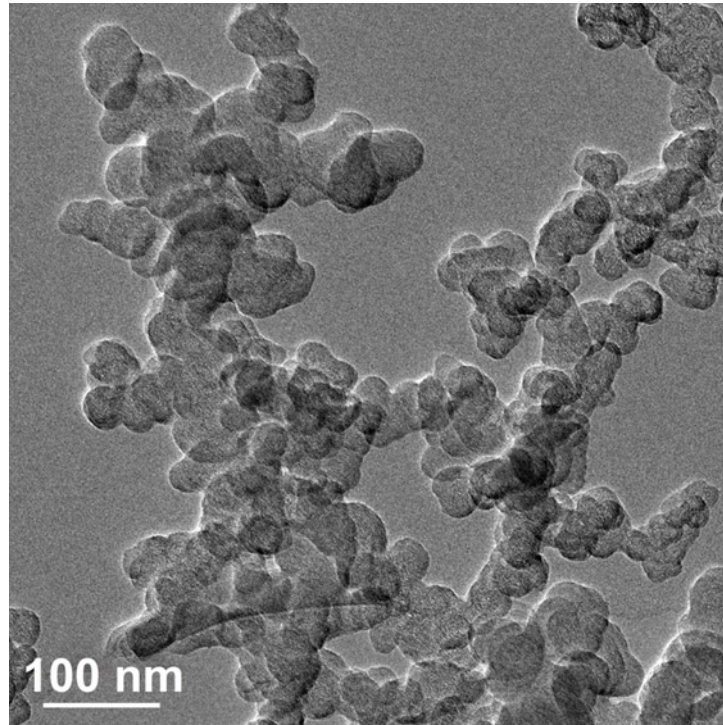


Fig. S31 TEM of carbon black (CB).

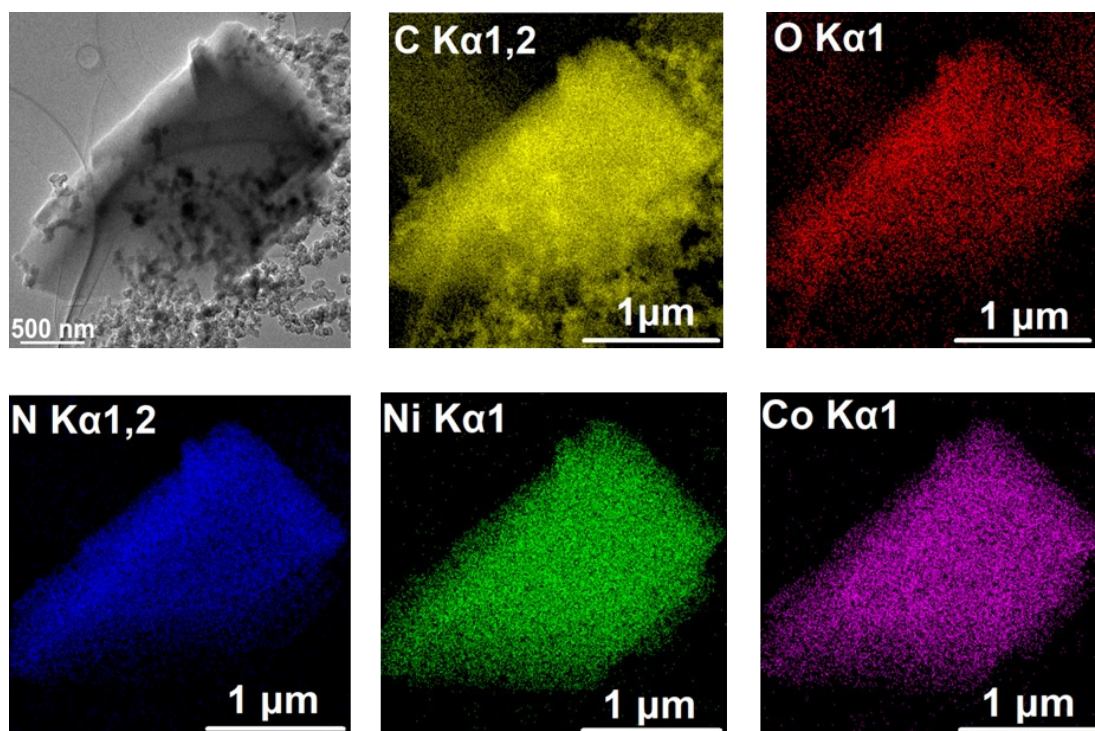


Fig. S32 TEM and element mapping of $\text{Ni}_{0.6}\text{Co}_{0.4}\text{-MOF NHs/CB}$.

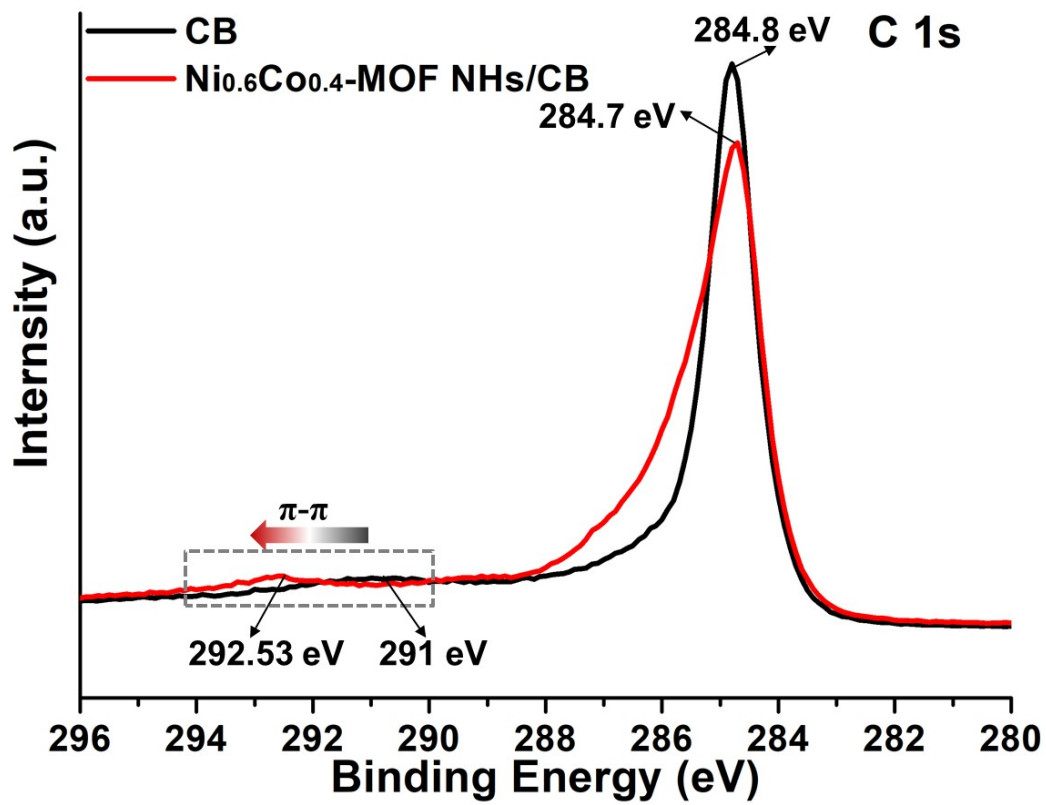


Fig. S33 XPS fine spectra of C 1s for CB and Ni_{0.6}Co_{0.4}-MOF NHs/CB.

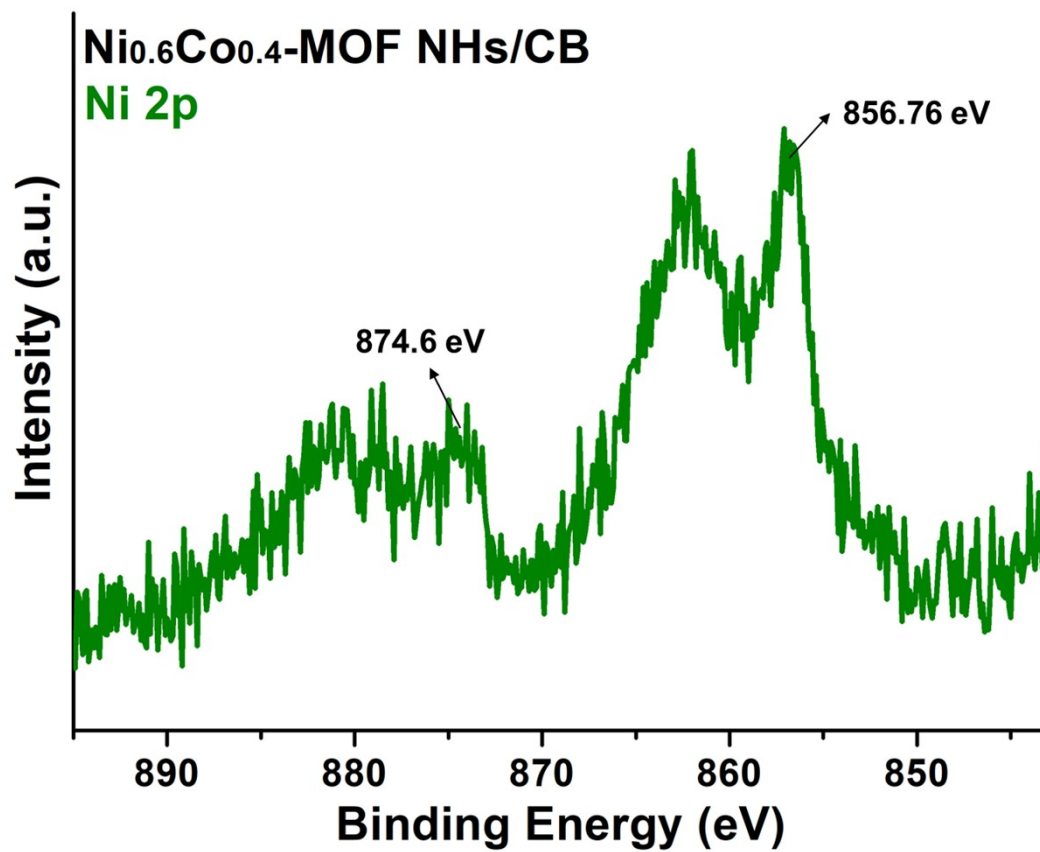


Fig. S34 XPS fine spectra of Ni 2p for Ni_{0.6}Co_{0.4}-MOF NHs/CB.

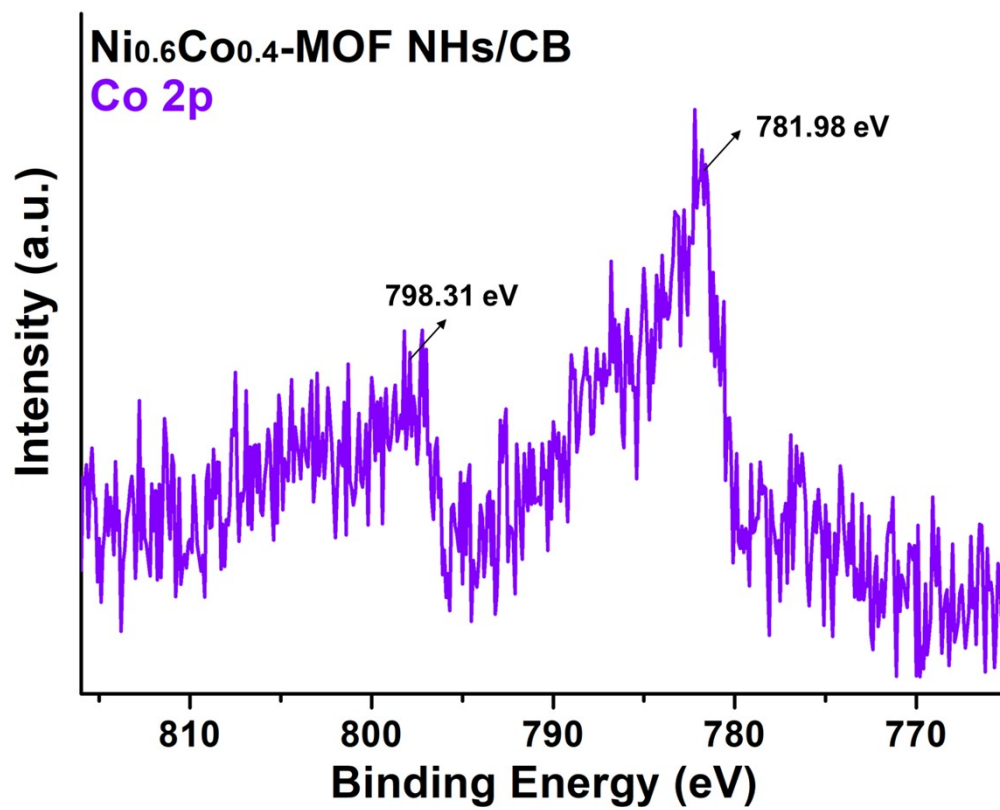


Fig. S35 XPS fine spectra of Co 2p for Ni_{0.6}Co_{0.4}-MOF NHs/CB.

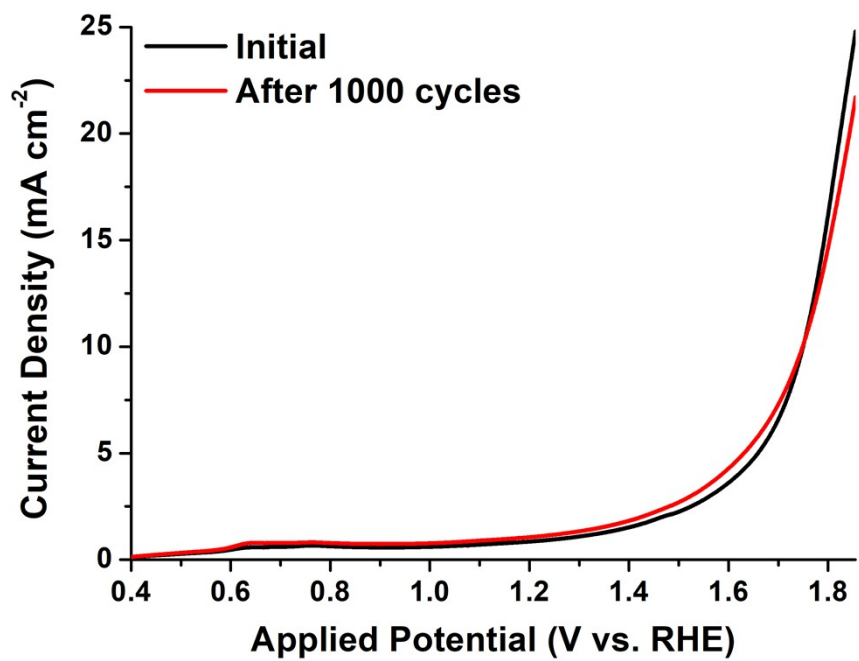


Fig. S36 Stability tests of Ni_{0.6}Co_{0.4}-MOF NHs/CB before and after 1000 cyclic potential scans in 0.05 M H₂SO₄.

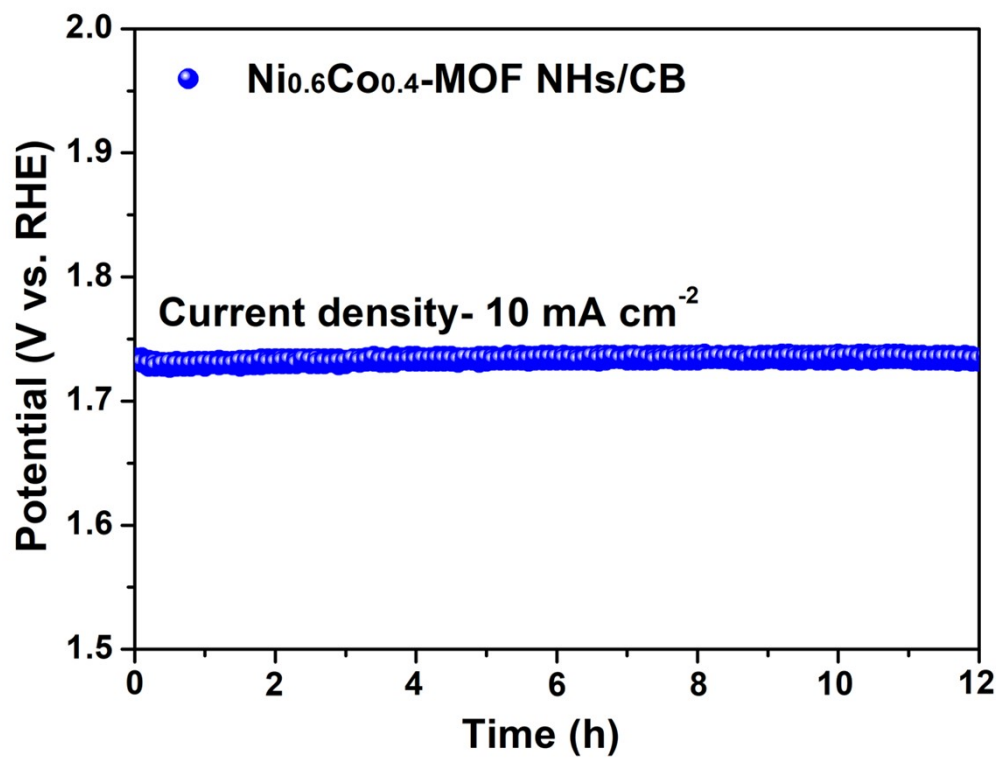


Fig. S37 Chronopotentiometry of $\text{Ni}_{0.6}\text{Co}_{0.4}\text{-MOF NHs/CB}$.

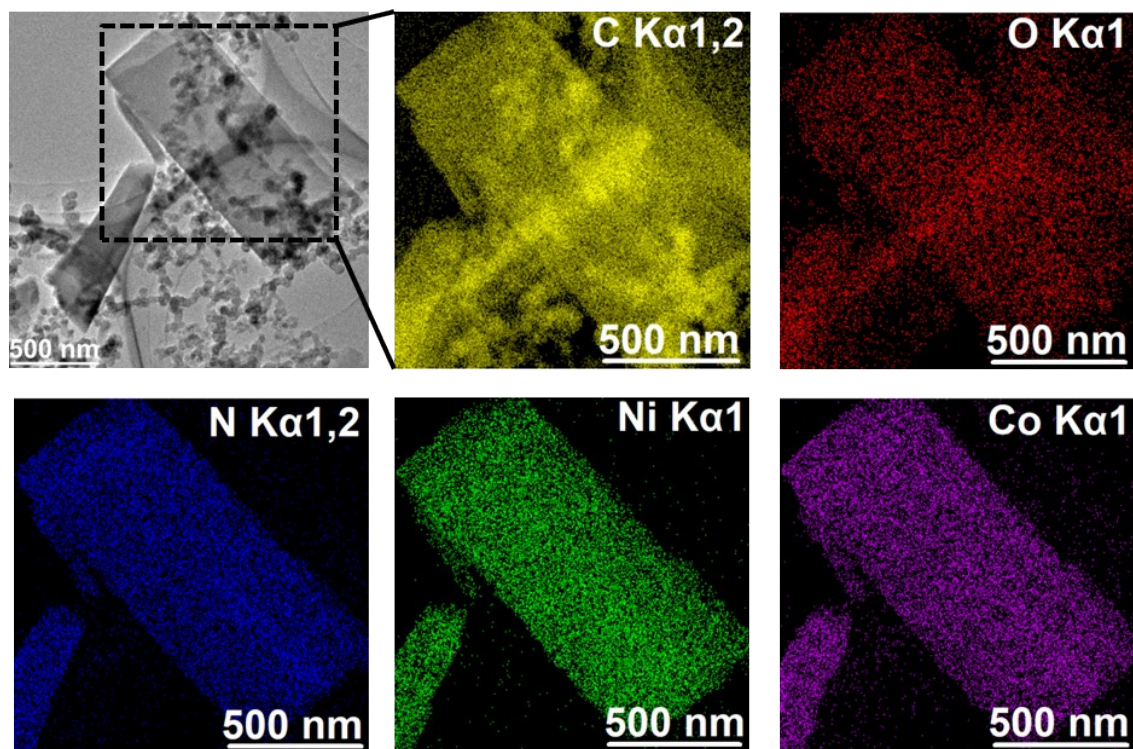


Fig. S38 TEM and element mapping of $\text{Ni}_{0.6}\text{Co}_{0.4}\text{-MOF NHs/CB}$ after OER testing.

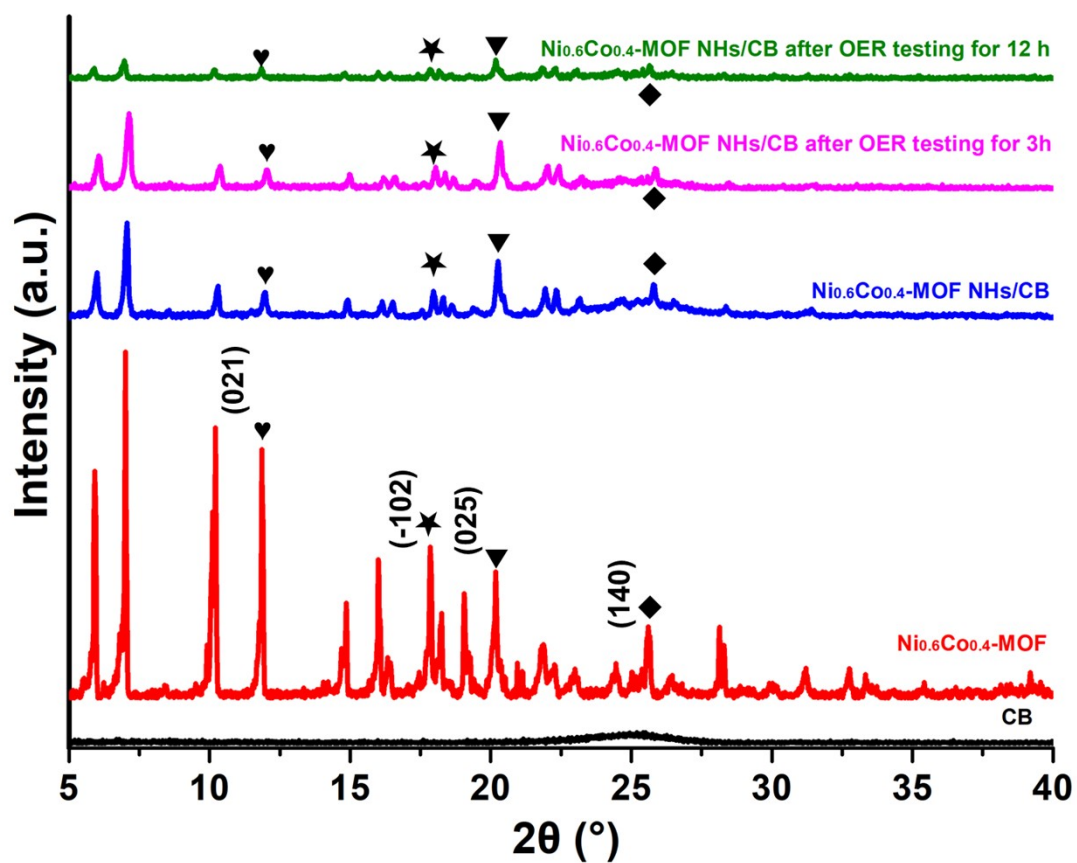


Fig. S39 XRD patterns of CB, Ni_{0.6}Co_{0.4}-MOF/CB and Ni_{0.6}Co_{0.4}-MOF/CB obtained at different OER test time (3 h and 12h).

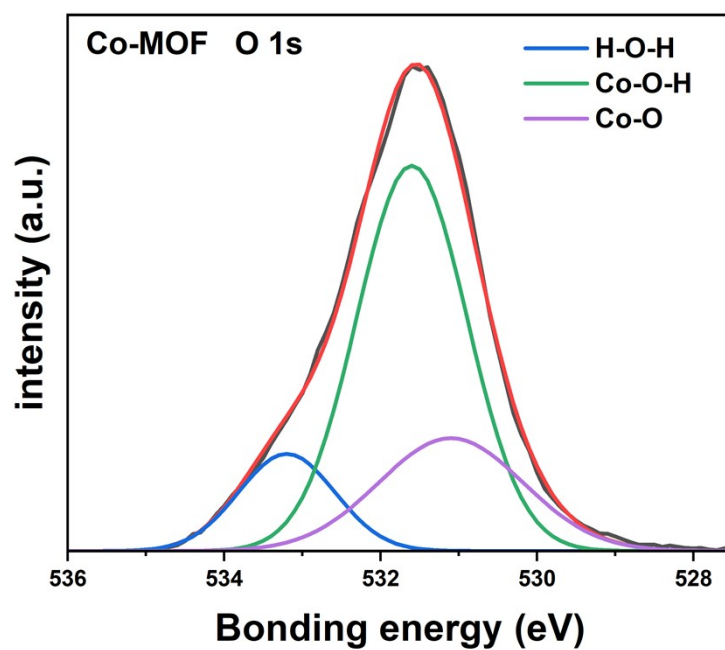


Figure S40 The characterization results of Co-MOF O1s XPS spectra.

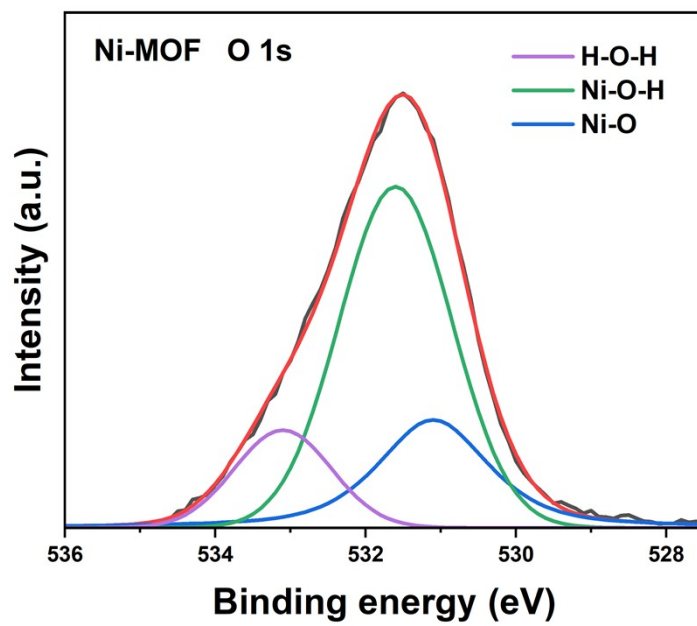


Fig. S41 The characterization results of Ni-MOF O 1s XPS spectra.

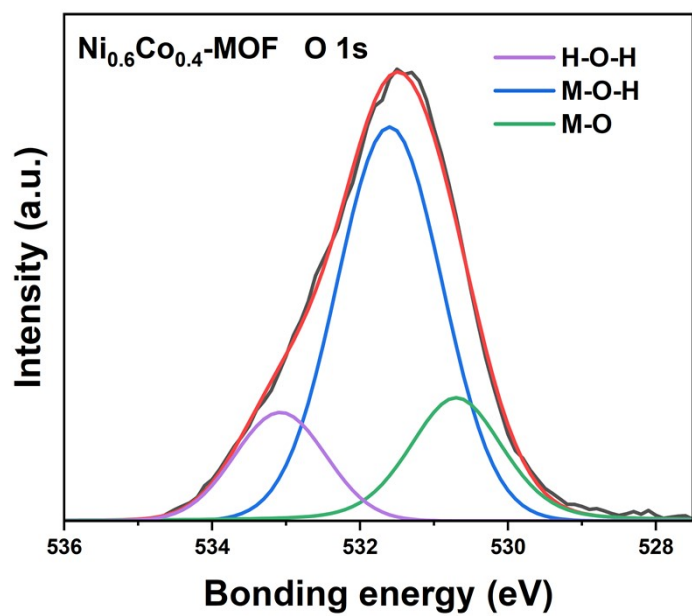


Fig. S42 The characterization results of Ni_{0.6}Co_{0.4}-MOF O 1s XPS spectra.

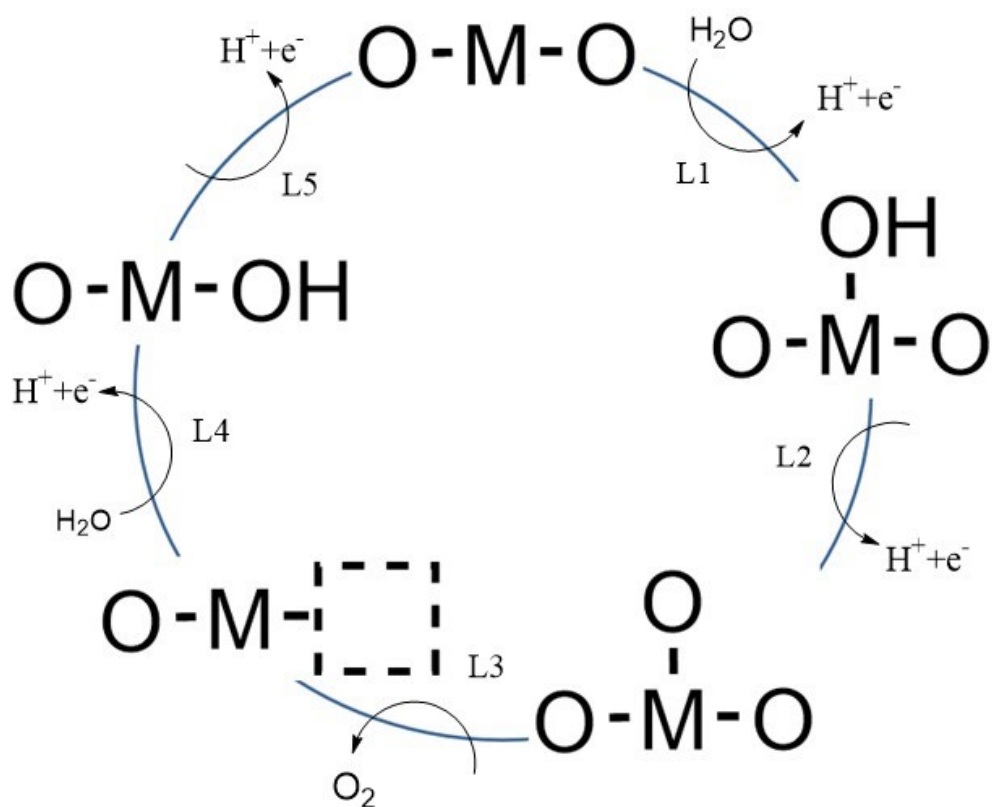
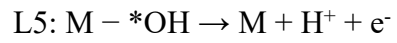
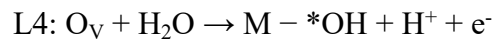
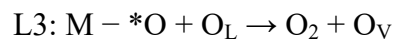
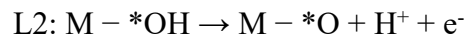


Fig. S43 Schematic diagram of LOM catalytic mechanism.

During the entire water oxidation process, a water molecule is first adsorbed on the catalyst ($Ni_{0.6}Co_{0.4}$ -MOF NHs/CB) surface and oxidized to form *OH (L1), and then loses a pair of electrons and protons to form *O (L2). During the OER process, oxygen in the lattice can detach from the MOF surface and form further peroxides with water molecules or metal oxygen intermediates. The generated intermediates combine on the $Ni_{0.6}Co_{0.4}$ -MOF NHs/CB surface to form oxygen molecules (L3), which desorb into the gas phase. This process involves the release of lattice oxygen and the formation and desorption of oxygen molecules. Afterwards, defects of oxygen vacancies are generated in the $Ni_{0.6}Co_{0.4}$ -MOF NHs/CB structure. Finally, through the dissociation of water or the re adsorption of lattice oxygen, the generated oxygen vacancies are refilled with *OH , which further oxidizes and returns to the initial state of the oxide catalyst.



(where O_V is an oxygen vacancy, O_L is free lattice oxygen)

- S1 J. Fan and B. E. Hanson, *Chem. Commun.*, 2005, 2327-2329
- S2 D. J. Ashworth, T. M. Roseveare, A. Schneemann, M. Flint, I. D. Bernaldes, P. Vervoorts, R. A. Fischer, L. Brammer and Jonathan A. Foster, *Inorg. Chem.*, 2019, 58, 10837-10845.
- S3 G. Che, Y. Zhao, W. Yang, Q. Zhou, X. Li, Q. Pan and Z. Su, *Inorg. Chem.*, 2024, 63, 10767-10774.
- S4 D. J. Ashworth and J. A. Foster, *Nanoscale*, 2020, 12, 7986.
- S5 G. Qin, J. Wang, L. Li, F. Yuan, Q. Zha, W. Bai and Y. Ni, *Talanta*, 2021, 221, 121421.
- S6 Q. Xia, J. Yang, S. Zhang, J. Zhang, Z. Li, J. Wang and X. Chen, *J. Am. Chem. Soc.* 2023, 145, 6123-6134.
- S7 C. Tan, K. Yang, J. Dong, Y. Liu, Y. Liu, Jianwen Jiang and Yong Cui, *J. Am. Chem. Soc.* 2019, 141, 17685-17695.
- S8 D. J. Ashworth, A. Cooper, M. Trueman, R. W. M. A.-Saedi, L. D. Smith, A. J. H. M. Meijer, and J. A. Foster, *Chem. Eur. J.* 2018, 24, 17986-17996.
- S9 N. C.-Pereda, F. Moghzi, J. Baselga, H. Zhong, Jan Janczak, J. Soleimannejad, R. Dong and D. R.-Molina, *Ultrason. Sonochem.* 2021, 70, 105292.
- S10 F.-F. Wang, Z. Liu and Z.-L. Cheng, *Appl Organomet Chem.* 2020;34:e5950.